# Block Copolymer Micelles for Drug Delivery

Andreia Filipa Fidalgo de Sousa

Thesis to obtain the Master of Science Degree in

**Chemical Engineering**

Supervisor(s): Doctor Célia Maria da Cruz Fernandes

Doctor Francisco França Alcântara Conceição Silva

**Examination Committee**

Chairperson: Professor Maria Matilde Soares Duarte Marques

Committee Member: Doctor Fernanda Marujo Marques

Supervisor: Doctor Célia Maria da Cruz Fernandes

**January 2021**

The work presented in this thesis was performed at the Radiopharmaceutical Sciences Group of the Center of Nuclear Sciences and Technologies ($C^2TN$) of Instituto Superior Técnico (IST) (Lisbon, Portugal), under the supervision of Doctor Célia Fernandes and Doctor Francisco Silva.

# Acknowledgments

First, I would like to thank Doctor Célia Fernandes and Doctor Francisco Silva for the opportunity to do my master's thesis on two subjects that I love: Biochemistry and Chemical Engineering and for all the help that they provided me during the months in the laboratory.

I would also like to thank my mother, father and brother for all the support during the most difficult times and for believing in me.

And finally, without my friends I would have given up, so thank you André, Rita, José, Inês, Kilian, Tânia and Rúben for all the support and all the kind words.

# Resumo

Vários complexos de ouro foram estudados para desenvolver potenciais agentes quimioterapêuticos. Contudo, uma baixa solubilidade em água dificulta a sua ação *in vivo*. Micelas poliméricas, têm a capacidade de solubilizar fármacos hidrofóbicos no interior do seu núcleo hidrofóbico aumentando o tempo de circulação na corrente sanguínea. O objetivo do trabalho desenvolvido nesta tese era proporcionar solubilidade em água, circulação biológica prolongada e consequentemente, uma melhor capacidade terapêutica ao complexo de ouro $[Au(cdc)_2]^-$ (cdc = cianoditioimido carbonato) através do seu encapsulamento em micelas poliméricas.

As micelas carregadas, BCM-$[Au(cdc)_2]$, foram sintetizadas com uma eficiência de carga de 64,59% e um teor de carga de 35,29 $mg_{cdc}/g_{BCM}$. O diâmetro hidrodinâmico (Dh) e o potencial zeta (Zp) foram determinados por DLS e LDV, respetivamente, concluindo-se que a amostra era homogénea e que as micelas são boas candidatas para a entrega de fármacos, pois $d_h$ = 77,31 ± 27,00 nm e PdI = 0.18 (índice de polidispersidade baixo). Ademais, o potencial zeta (-57,20 ± 12,10 mV) sugere alta estabilidade das micelas.

Estudos de atividade citotóxica em células cancerígenas A2780 do ovário demonstraram que as BCM-$[Au(cdc)_2]$ mantiveram atividade citotóxica relevante comparável à observada para igual concentração de complexo de ouro.

As micelas foram radiomarcadas com $^{111}$In-oxina e $^{67}$Ga-oxina (alto rendimento radioquímico e elevada pureza (> 95%)). Estudos de estabilidade mostraram que as micelas marcadas, $^{111}$In-BCMs e $^{67}$Ga-BCMs, são estáveis em PBS pH 7.4, a 37°C (até 4 dias). Estudos de biodistribução com $^{67}$Ga-BCMs em ratinhos CD1 saudáveis mostraram uma vida útil prolongada de circulação na corrente sanguínea.

**Palavras-chave:** micelas poliméricas, entrega de fármacos, teor de carregamento, radiomarcação, biodistribuição

# Abstract

Recently, several gold bisdithiolate complexes were studied aiming to find potential chemotherapeutic agents. However, their poor water solubility may hamper their action *in vivo*. Polymeric micelles offer the opportunity to solubilize hydrophobic drugs in their hydrophobic core and improve their bioavailability and their circulation time in blood. In this context, the goal of this project was to provide water solubility, prolonged availability, and an enhanced therapeutic index to the gold complex $[Au(cdc)_2]^-$ (where cdc = cyanodithioimido carbonate) loaded in polymeric micelles for drug-delivery.

Given so, loaded micelles BCM-$[Au(cdc)_2]$ were synthesized and characterized. The BCM-$[Au(cdc)_2]$ were prepared with a loading efficiency of 64.59% and a loading content of 35.29 $mg_{cdc}/g_{BCM}$. The hydrodynamic diameter ($D_h$) and the zeta potential (Zp) of the micelles were determined by DLS and LDV, respectively. A $D_h$ of 77.31 ± 27.00 nm and a low polidispersity index (PdI) of 0.18, were determined indicating the sample were homogenous and the micelles are good candidates for drug delivery. The zeta potential (-57.20 ± 12.10 mV) suggests high stability of the micelles.

Cytotoxic activity studies against the ovarian A2780 cancer cells, have shown that $[Au(cdc)_2]$-loaded BCMs maintain relevant cytotoxic activity comparable to the cytotoxicity observed for the same concentration of gold complex.

The micelles were radiolabeled with $^{111}$In-oxine and $^{67}$Ga-oxine in high radiochemical yield and purity (> 95%) affording $^{111}$In-BCMs and $^{67}$Ga-BCMs stable in PBS pH 7.4, at 37°C for at least 4 days. Biodistribution studies with $^{67}$Ga-BCMs in healthy CD1 mice has shown prolonged circulation lifetime in the bloodstream.



**Key words:** polymeric micelles, drug delivery, loading content, radiolabeled micelles, biodistribution

# Table of Contents

# List of Tables

# List of Figures

# List of Abbreviations

**PK** – Pharmacokinetics

**RES** – Reticuloendothelial Systems

**PEG** – Polyethylene Glycol

**PCL** – Poly(*ε*-caprolactone)

**CMC** – Critical Micelle Concentration

**PM** – Polymeric Micelles

**THF** – Tetrahydrofuran

**CDC** – Cyanodithioimido Carbonate

**ACN** – Acetonitrile

**DMF** – N-dimethylformamide

**DMSO** – Dimethylsulfoxide

**HPLC** – High-Performance Liquid Chromatography

**LC** – Loading Content

**LE** – Loading Efficiency

**BCM** – Block Copolymer Micelles

**EPR** – Enhanced Permeability and Retention

**MPS** – Mononuclear Phagocytic System

**EGFR** – Epidermal Growth Factor Receptor

**NI** – Nuclear Imaging

**CT** – Computed Tomography

**MRI** – Magnetic Resonance Imaging

**DLS** – Dynamic Light Scattering

**ZDV** – Laser Doppler Velocimetry

**$D_h$** – Hydrodynamic Diameter

**PdI** – Polydispersity Index

# 1 Introduction

## 1.1 Nanotechnology and Drug Delivery

One of the main focus of nanotechnology application in the medical field is to provide more effective methodologies and tools for drug delivery in order to overcome their inherent limitations and drawbacks that hinder their required effectiveness and pharmacological efficacy.[1] Particularly, nanotechnology can be used for the design of drug delivery platforms with reduced toxicity while maintaining therapeutic effects, greater biocompatibility and safety[2]. This is accomplished by improving solubility, biodistribution and pharmacokinetics (PK), while also reducing non-selective activity for the targeted tissues, dose-limiting toxicity, multi-drug resistance, and fast degradation in the harsh *in vivo* environment.[3,4]

Nanoparticles are used in the delivery of drugs for the treatment of certain pathologies – such as malaria, bacterial infections and cancer – since they can overcome the possible resistance of the pathogenic agents towards drugs and the nonspecific target of the tumours cell [5]. However, this is not the only application of the nanostructures. Nanomedicine is also used for gene delivery, *in vivo* and *in vitro* diagnosis, vaccine development, *in vivo* medical imaging, systems and devices for nanotherapeutics and for the functionalization of biomaterials for regenerative medicine[2,6,7]

Nanoparticles, also designated nanocarriers in the case of drug delivery platforms, can have a size range from 1 to 100 nm[1], and include a variety of nanoscale systems such as polymeric and metallic nanoparticles, polymeric micelles, liposomes, dendrimers, nanogels, nanocapsules, carbon nanotubes, nanocrystals and solid lipid nanoparticles[3] (Figure 1[8] ).

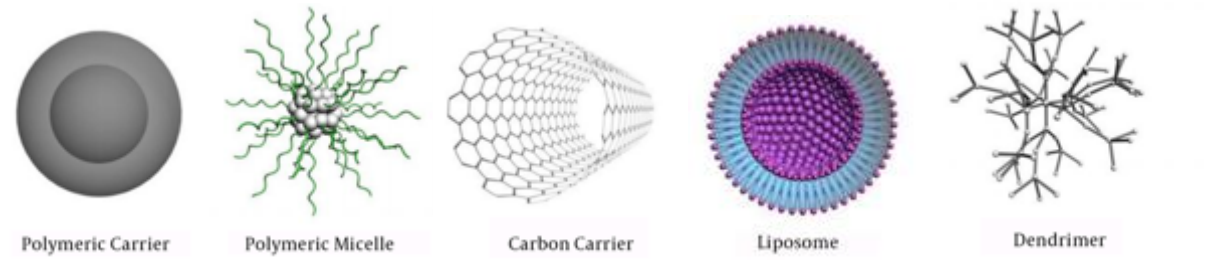


**Figure 1 – Examples of nanoscale systems.**

Nanocarriers generally have a prolonged *in vivo* circulation half-life, increase of drug stability, and the ability to solubilize hydrophilic and hydrophobic agents to precisely deliver them to the targeted diseased cells and tissues. Additionally, they can also be designed to react to several external and internal stimuli for “triggered” release to achieve spatial and temporal control over the unloading of therapeutic payload. This can be achieved by chemical modification of the nanoparticle structure. [1,3] (Table 1).

**Table 1 – Advantages and disadvantages of different types of nanocarriers.**[9]

| Types of Carriers | Advantages | Disadvantages |
|---|---|---|
| Liposomes | Biocompatible<br>Longer duration of circulation<br>Amphiphilic | May trigger immune response |
| Carbon nanoparticles | Multiple functions<br>Chemical modification<br>Water soluble and biocompatible<br>Efficient loading | Toxicity |
| Polymeric micelles | Efficient carrier system for hydrophilic drug<br>Biodegradable, self-assembling and biocompatible<br>Potential targeting<br>Functional modification | Occasional cytotoxicity<br>Need of surface modifications |
| Dendrimers | Uniformity in size, shape and branch length<br>Tuned pharmacokinetics and biodistribution<br>Increased surface area, increased loading<br>Targeting is achieved | Complex synthetic route |
| Metallic nanoparticles<br>Gold nanoshells | Uniformity in size, shape and branch length<br>Tuned pharmacokinetics and biodistribution<br>Increased surface area, increased loading<br>Targeting is achieved | Toxicity |

However, there are also some disadvantages associated with the use of nanoparticles, one of the most common is the toxicity of some of the types of nanostructures. It is therefore important to take into consideration that material properties differ significantly at the nanoscale range, with the increased surface-to-volume ratios, leading to an increased reactivity[10] and altered surface chemistry[3]. Therefore, some factors must be considered for safety concerns in the design of nanocarriers. These factors

include the dose or concentration of the nanocarriers, their material of composition, the size, surface charge, shape and reactivity and solubility.

In order to understand why the design must take into consideration the factors mentioned before, it is necessary to define the administrative routes of nanoparticles – direct injection, inhalation and oral intake – and understand how the body handles the exogenous particulate matter. When the nanocarriers enter systemic circulation, the first phenomenon that takes place is the interaction of particle protein and the second one is the distribution into various organs. After that, the lymphatic system is responsible for the elimination of particles through absorption from the blood capillaries. The functions of the lymphatic system include the fluid recovery, which involves the filtering of fluids by this system, and the production of immune cells. This last function is very relevant in the design of nanomedicines for drug delivery since nanoparticles are known to be engulfed by macrophages to clear them from the body[11]. Besides the macrophages, opsonins, which facilitate the recognition of nanocarriers and elimination from the bloodstream by the reticuloendothelial systems (RES), are also a feature to take into consideration when designing novel nanoplatforms (Figure 2). A common way to overcome this issue is through modification of the nanocarriers with biocompatible materials like polyethylene glycol (PEG), for example. The use of PEG on the nanoparticle structure leads to a decreased adsorption by opsonin proteins and as consequence avoids phagocytosis[4].

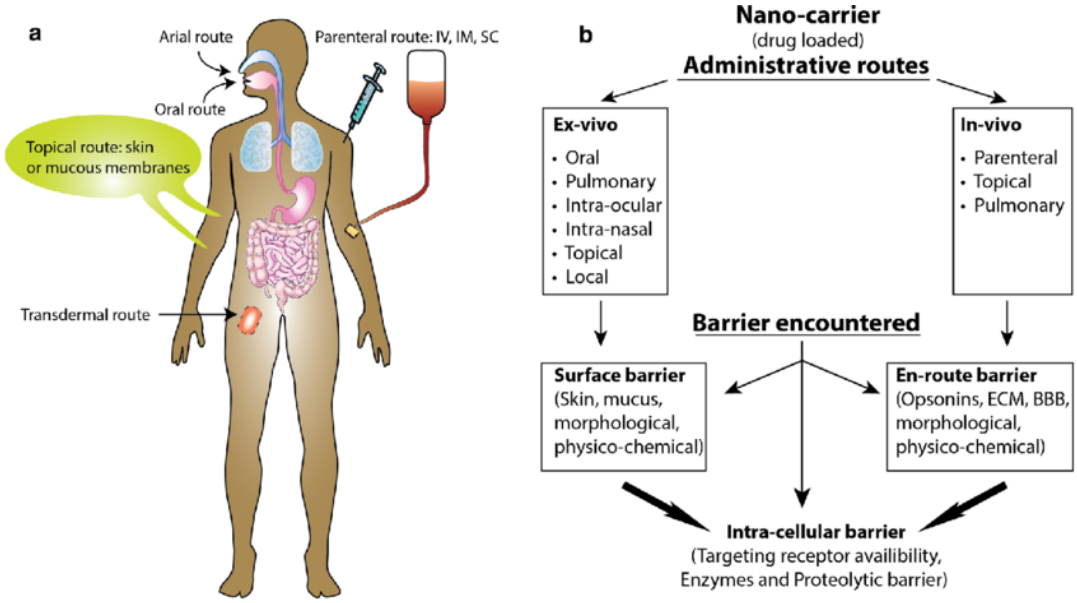


**Figure 2 – Administrative routes and barrier encounters for nanoparticles[12].**

Furthermore, biodistribution of nanocarriers can be affected by size and surface charge. Nanomedicines larger than 150 nm are retained in the spleen, while at sizes smaller than 150 nm they tend to accumulate in the liver. Also, it has been shown that nanocarriers 200 nm or larger are rapidly removed from circulation by the lymphatic system. The optimal size of these particles is less than 100 nm, as mentioned before. Nanomedicines with a positive charge are quickly sequestered in the spleen, liver and lungs, whereas nanocarriers with neutral or slightly negative charge have a prolonged circulation in the bloodstream, because they have a lower opsonization rate when compared to the positive charge ones.[2–4]

## 1.2 Polymeric Nanocarriers

### 1.2.1 Polymeric Micelles (PMs)

Polymeric micelles are nanometric particles of core–shell structures that are formed by the self-assembly of amphiphilic block copolymers composed of hydrophilic and hydrophobic segments. The selection of the polymer has an important role in the formation of micelles, and it is based on the characteristics of both hydrophilic and hydrophobic moieties of the block copolymers. The hydrophilic shell of the micelles has an important role because provides steric stability and prolongs the circulation time in the body of micelles, because when chosen properly avoids the quick uptake by the RES. The most used hydrophilic polymer is PEG, which is highly hydrated, water soluble and biocompatibility and has a low toxicity, but others can be also used such as polyethylene oxide, polysorbate 80, poloxamine and polyoxamer[9,13]. On the other hand, the hydrophobic block copolymer should have a good compatibility of the hydrophobic core with the incorporated drug and a high drug loading capacity. Polyesters, polyamino acids and polyethers are the most common polymers used for the formation of the hydrophobic core[4,13] In addition, PMs have different patterns depending on the arrangement of the block copolymers. There are three types of arrangement: (1) diblock copolymers (A-B type copolymers), (2) triblock copolymers (A-B-C type copolymer) and (3) grafted polymers[9,13].

The process of PM formation by self-assembly of the amphiphilic block copolymers in an aqueous media (Figure 3[3]) is entropically favoured, because of the dehydration of the hydrophobic tails of the amphiphilic monomers, and occurs above the critical micelle concentration (CMC), which is the lowest concentration of copolymer required to obtain micelles with a core-shell structure. Additionally, the micelle core is formed by hydrophobic polymers that are able to interact due to the formation of Van der Waals bonds, and the hydrophilic shell, also known as hydrophilic corona, re-establishes hydrogen bond networks with the adjacent water[3,13].The CMC of PMs depends on the molecular weight and type of the hydrophobic block. In general, the higher the molecular weight and the more hydrophobic, the lower the CMC, which leads to a greater stability even at low concentrations of the amphiphilic copolymers in the medium[3,13].

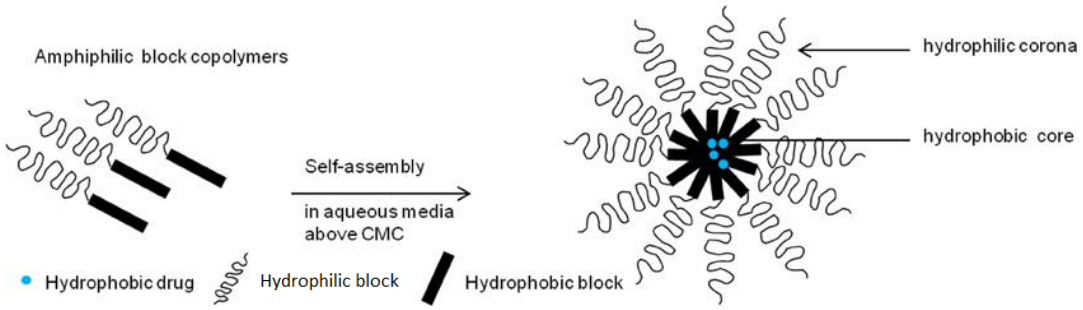


**Figure 3 – Self-assembly of amphiphilic block copolymers in aqueous media.**

The particular advantages of PMs for drug delivery are the following: (1) their ability to solubilize hydrophobic drugs or poorly water soluble within their core, thus enhancing their bioavailability; (2) their hydrophilic corona provides longer duration of circulation time inside the body, prevents a quick uptake of the formulation by RES and gives steric stability; (3) their biocompatibility; and (4) their low toxicity[3,9,13,14].

The drug loading of PMs can occur by two routes using amphiphilic monomers: (1) drug encapsulation, in which the drugs are physically entrapped into the hydrophobic core, and (2) drug conjugation, which uses a non-water-soluble drug as a hydrophobic core of micelles that are conjugated to the hydrophilic polymer backbone. In this last method, it is typically necessary to use biodegradable chemical linkers for the conjugation of the drug to the main chain in order to allow for the drug release in vivo[9].

#### 1.2.1.1 Synthesis of PMs

PMs can be prepared by five different methods such as direct dissolution, dialysis, oil in water emulsion, solvent evaporation and lyophilization, which are represented in Figure 4. The choice of the method is based on the extent of the solubility of the block copolymer in an aqueous medium[15].

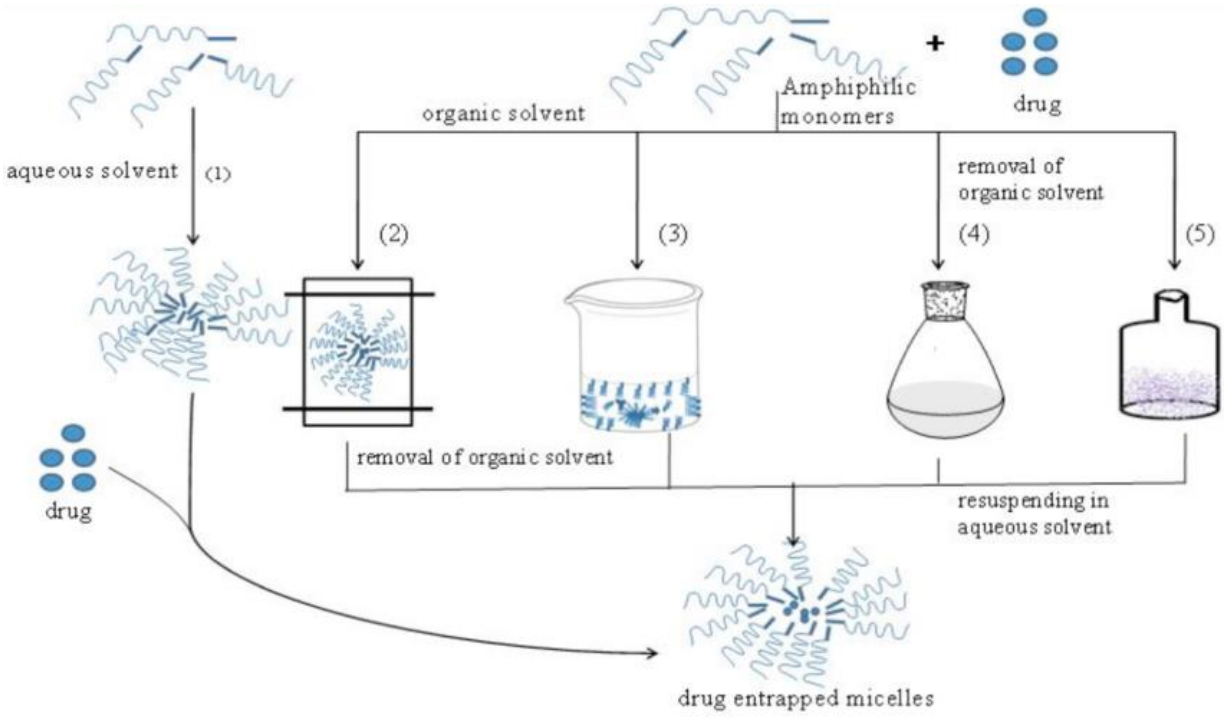


**Figure 4 – Methods for micelles preparation: (1) direct dissolution, (2) dialysis, (3) oil in water emulsion, (4) solvent evaporation. The lyophilization or freeze drying, (5), can also be used with other methods, since it is a way to save the polymer and the drug after the dissolution and use it for future studies, after the reconstitution with an aqueous solvent[15].**

The direct dissolution method is used for micelle preparation from copolymers with relatively high water solubility, because the drug and the polymer are directly dissolved in an aqueous media, which can be a buffer or distilled deionized water. The drug loading occurs by stirring, heating and/or sonication of the solution and the micelle formation occurs by dehydration of the core forming blocks[15]. Also, the low drug loading is one problem that this method faces and in order to overcome it, it is

necessary to apply this method with increasing temperature or by the preparation of a thin evaporated film of the drug before the addition of the copolymer[14].

On the other hand, the dialysis method is used when micelles are prepared from amphiphilic copolymers with low water solubility, so an organic solvent – acetone, tetrahydrofuran (THF), acetonitrile (ACN), N, N-dimethylformamide (DMF) or dimethylsulfoxide (DMSO) – is required for the solubilization to happen. In this method, the drug and the copolymer are dissolved in an organic solvent and the formation of micelles is stimulated by the addition of water to the drug-copolymer mixture. Then, micelles are dialyzed for the organic solvent to be replaced by water. Moreover, the choice of solvent influences the physical and drug encapsulation properties of the micelles. In addition, the size, drug loading capacity and stability of micelles may be influenced by the optimal aqueous to organic solvent ratio[14,15].

In the solvent evaporation method, both the drug and the copolymer are dissolved in a common solvent or mixture of two miscible solvents. Then, a drug-copolymer film is formed upon stirring and drying the mixture (by a flow of $N_2$ or at room temperature). Micelles are formed when the film is reconstituted with water or buffer. In order to prevent a multimodal size distribution, the reconstituted micelles may be sonicated or passed through a high-pressure extruder. The drug encapsulation is determined by the solvent employed for the dissolution of both the drug and the copolymer[15]. This method was the one chosen for the studies conducted during this thesis.

Finally, another method is where the copolymer and the active agent are dissolved in a mixture of aqueous and organic solvent, followed by lyophilisation, and then the freeze-dried sample can be reconstituted in order to obtain the drug-loaded micelles. The solvents used are mainly *tert*-butanol and dimethylacetamide because they have a high vapour pressure, offering rapid sublimation followed by lyophilization. The micelles produced demonstrate a high water dispersibility and an adequate shelf-life[15].

#### 1.2.1.2 Passive Targeting of PMs

The delivery of drugs to tumour sites is commonly based on the phenomenon of passive targeting, by exploiting the pathophysiological and anatomical abnormalities of the tumour vasculature and uses the enhanced permeability and retention (EPR) effect[16] (Figure 5).The EPR effect is one of the main factors associated with the greater accumulation of nanoparticles in tumour tissues than in normal tissues. This happens because tumour vasculature grows abnormally to meet the high demand of oxygen and nutrients of the growing tumour, which leaves the endothelial cells poorly aligned with large fenestrations between them; together with the production of vascular permeability factors – nitric oxide, vascular endothelial growth factor, bradykinin and matrix metalloproteinases – it makes the tumour blood vessels extremely permeable. This phenomenon allows the leakage of plasma components, such as nanoparticles and macromolecules, into the tumour tissues. Also, the tumours have a poor lymphatic drainage, because tumours cells compress the lymph vessels causing their collapse, that allows the nanoparticles to be retained in the tumour tissues, thus facilitating the sustained release of their drugs[3,16].

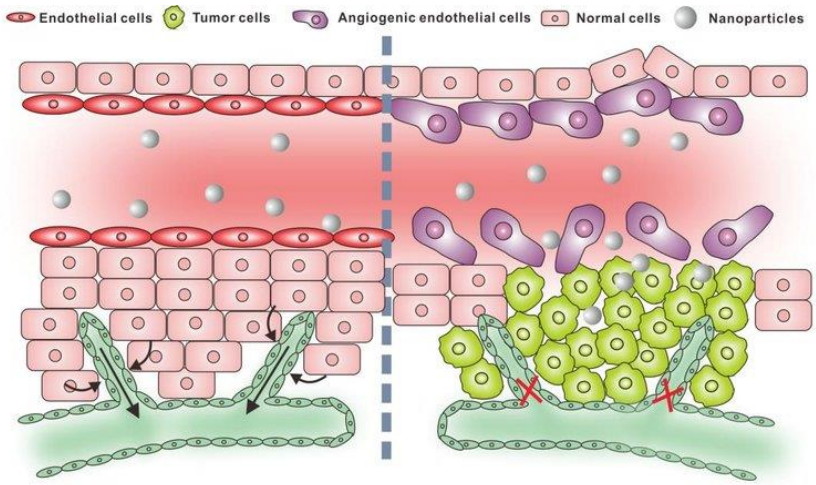


**Figure 5 – Schematic illustration of the EPR effect[17].**

The effectiveness of the passive targeting can be determined by the surface characteristics and size of micelles. The size of polymeric micelles is important due to the cut-off sizes of tumour vasculature, which can vary between 200 – 800 nm, since their size must be below the cut-off size in order to remain in circulation for longer intervals without being taken up by the mononuclear phagocytic system (MPS) and enter the tumour tissues through the EPR effect[3]. In addition, most of the passive targeting polymeric micelles have a surface covered with PEG for biocompatibility and because it is effective in preventing quick opsonization of micelles by the MPS, as mentioned before[3,14].

There are, however, limitations with passive targeting: (1) the nonspecific uptake and delivery of the nanocarriers and (2) the presence of mucosal barriers, which are the primary defence mechanism of the organisms, trapping and removing bacteria, viruses, micro and nano-sized particles[14,18].

In order to overcome these issues, in particular nonspecific delivery of the nanoparticles, active targeting methodologies are used.

#### 1.2.1.3 Active Targeting of PMs

Tumour cells normally show an enlarged expression of determined antigens or receptors, such as EGFR (epidermal growth factor receptor), that are not expressed or are expressed at low levels in the surface of normal cells[3,19]. The specific interactions (covalent or noncovalent) between the polymeric micelle and receptors or antigens on the target cell, which can also promote the internalization of nanocarriers trough receptor-mediated endocytosis, are the basis of active targeting[9,20].

The efficiency and the targetability of the uptake depend on the interactions between the plasma membrane antigens/receptors and the nanocarrier surface, which is linked to the density of the receptors/antigens and the ligands present on the cell and the polymeric micelle, respectively. The targeting ligands can be vitamins (vitamin D), proteins (lectins, transferrin), monoclonal antibodies (anti-Her2, anti-EGFR), peptides (Arg-Gly-Asp or RGD), aptamers (RNA aptamers against HIV glycoprotein), or carbohydrates (galactose)[9,20] (Figure 6).

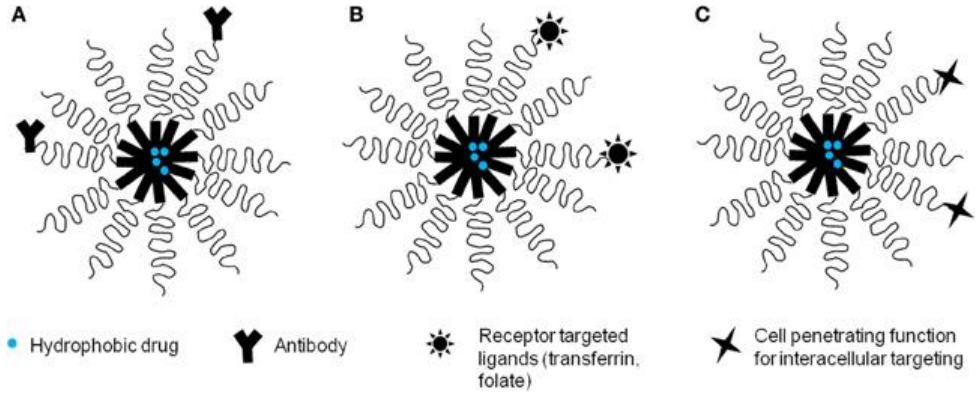


**Figure 6 – Drug-loaded polymeric micelles with a variety of targeting functions: (A) antibody-targeted micelles, (B) ligand-targeted micelles, and (C) micelles with the function of cell-penetrating[3].**

In general, the targeting ligand can be attached to the water-exposed free ends of hydrophilic blocks (e.g. PEG), which avoid steric hindrance when binding to their targeted receptors/antigens[3].Thus, active targeting has the following advantages over the passive targeting: (1) improving efficacy of drug delivery, since higher intracellular drug concentrations are obtained, (2) reducing systemic toxicity side effects, due to lower accumulation of the PMs in normal tissues[13,21].

#### 1.2.1.4 Multifunctional PMs

PMs can be modified in order to include (1) surface modification with ligands to allow for selectivity targeting and the intracellular delivery of drugs, (2) modifications that allow micelles to answer to a number of extrinsic and intrinsic stimuli for “triggered” drug release at diseases sites, (3) modifications that incorporate a dye for imaging, and (4) modifications for longevity, which is important for the passive targeting. Multiple modifications can be integrated within a single micelle.

The integration of various functions to the PMs can significantly increase their pharmacological efficacy. For instance, by incorporating imaging moieties in combination with the drug delivery capability of the PMs, it is possible to track the in vivo biological profile in the body and verify if they are being directed to the target area[13]. PMs are considered theranostic when they have moieties that enable them to sequentially or simultaneously perform diagnostic and therapeutic functions[3,16] (Figure 7).

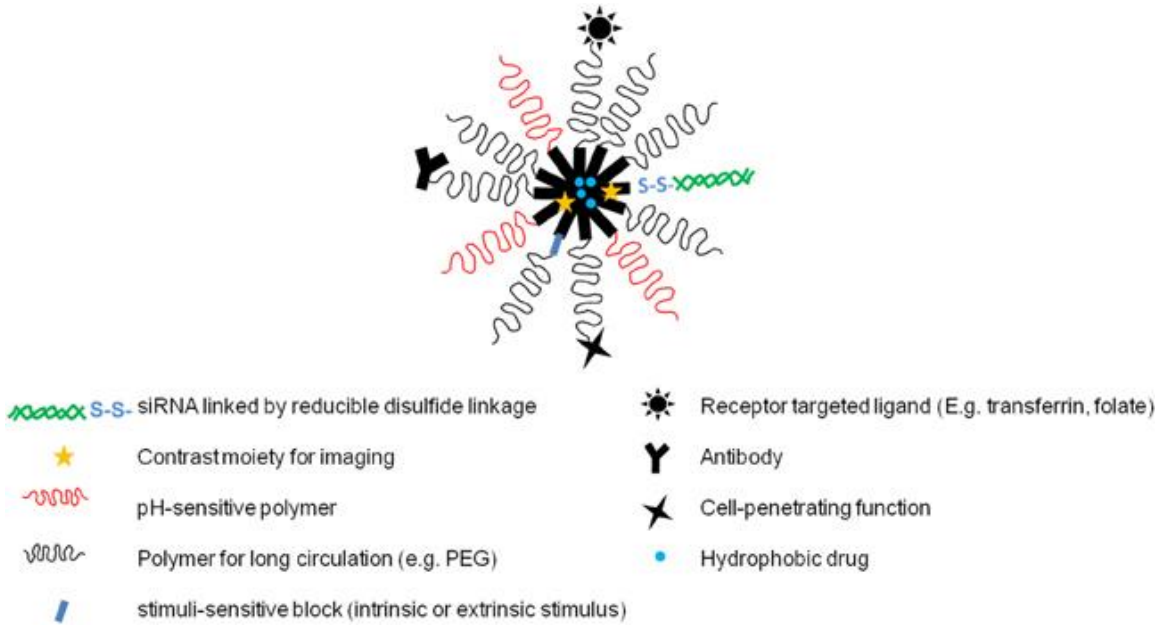


**Figure 7 – A hypothetical multifunctional polymeric micelle[3].**

PMs that are known as “environmental-responsive” or “smart” are stimuli-sensitive nanocarriers that have the capability to respond to various intra- and extracellular biological stimuli (acidic pH, altered redox potential, and upregulated enzyme), as well as artificial stimuli (magnetic field, light, temperature, and ultrasound) to achieve temporal and spatial control over the release of therapeutic payloads, which occurs when PMs undergo structural alterations – supramolecular aggregation, polymerization, isomerization or disintegration/destabilization. These nanocarriers can be used for drug delivery and imaging, which can play an important role in the diagnosis of cancer and therapy response evaluation[3,22,23] .

## 1.3 Polymeric Nanoparticles for Imaging Applications

As mentioned previously, polymeric nanoparticles can be used as pharmaceuticals for imaging in cancer diagnosis and/or therapy response evaluation. The incorporation of the imaging agent inside the polymeric nanoparticles, in addition to the drug agent, helps to monitor the localization and the pathway of these nanocarriers at the target site and the drug action to assess, in a non-invasive way, the therapeutic response and the tumour physiology (in the case of cancer therapeutics)[11,24], so it is possible to verify the biodistribution of the nanoparticle in real time, even in *in vivo* studies[22,24].

As described above, PMs display various advantages and disadvantages as nanocarriers for drug delivery, but the use of polymeric micelles as contrast agents has also some advantages associated such as the potential for cell tracking and targeted imaging applications and long blood-pool residence times[25].

The visual control of the drug delivery by nanoparticles can be achieved by different imaging techniques, including nuclear imaging, X-ray computed tomography (CT), magnetic resonance imaging (MRI) and ultrasonography, where micellar forms of contrast agents have been used[13,25].

### 1.3.1 Magnetic Resonance Imaging (MRI) vs Computed Tomography (CT)

MRI, which is more suitable for imaging of soft tissues, detects changes in the magnetization of hydrogen nuclei ($^{1}H$) in the body in a strong magnetic field after radiofrequency pulses are applied. The elements used as contrast agents are paramagnetic elements such as gadolinium, holmium, manganese and iron, since they alter the magnetization of hydrogen nuclei, resulting in the enhancement of contrast[13,26].

CT imaging uses the differences in absorption of X-rays between different tissues in the body to distinguish between structures in the body. The elements used as contrast agents are heavy ones such as bromine, iodine and barium. In addition, the concentration required of the contrast agent in the location of interest is approximately $10^{-2}$ M[13,26].

Comparing the two methods, MRI has a higher sensitivity since a lower concentration of the contrast agent is required at the local of interest. In addition, MRI is more appropriate for imaging of soft tissues.

### 1.3.2 Nuclear Imaging (NI)

The visualization of minute amounts of gamma-emitting or positron-emitting isotopes is allowed by nuclear imaging. In the case of the single photon emission computed tomography (SPECT) imaging, which refers to the gamma-emitting isotopes, iodine-123 ($^{123}I$), technetium-99m ($^{99m}Tc$) and indium-111 ($^{111}In$) are the isotopes used. On the other hand, fluorine-18 ($^{18}F$), copper-64 ($^{64}Cu$) and zirconium-89 ($^{89}Zr$) are the isotopes used for the positron emission tomography (PET) imaging, which refers to the positron-emitting isotopes. The isotope concentration required at the site of interest is approximately $10^{-10}$ M, so it is possible to conclude that nuclear imaging is the most sensitive imaging modality[13,26].

In comparison to the techniques mentioned before, NI is the most sensitive technique since is the one that needs the lowest concentration of the contrast agent[13].

## 1.4 Gold compounds for medical applications

Gold and gold compounds have been used in medicine since ancient times for the treatment of a wide variety of diseases[27]. Auranofin, is a gold(I) triethylphosphine compound approved by FDA for the treatment of rheumatoid arthritis but adverse side effects led to a significant decline in its clinical use[28,29]. Nevertheless, auranofin is currently being investigated for new therapeutic options like the treatment of some cancers, including leukaemia and ovarian cancer[30–32]. Besides auranofin, several gold compounds have been designed for medical applications[33,34]. Recently, less explored gold(III) complexes based on bisdithiolenes have emerged as potential anticancer and antimicrobial agents[35–37]. However, these complexes have poor solubility in water, which poses some challenges regarding their *in vivo* administration even though it is not a limiting factor. The association of these compounds with nano-sized carriers such as micelles, could circumvent the solubility issue and reduce ligand displacement reactions with blood proteins[11]. As mentioned above, further advantages of these nanoplatforms is their ability to change the pharmacokinetic and *in vivo* circulation time resulting in increased drug accumulation based on the EPR effect[16].

## 1.5 Objectives

Gold complexes are being largely studied for the treatment of various types of cancer, despite their poor solubility in water. In order to overcome this problem, polymeric micelles can be used since they encapsulate hydrophobic compounds and are vehicles for drug delivery. Also, polymeric micelles can be multifunctional since they can incorporate radioactive isotopes, in addition to the encapsulation of the compound. Having that in mind, the work developed in this thesis had the following main objectives: (1): study the efficiency of encapsulation of $[Au(cdc)_2]^-$, by polymeric micelles using UV-Vis Spectroscopy; (2) determine the cytotoxicity of the polymeric micelles with the $[Au(cdc)_2]^-$ encapsulated; (3) produce multifunctional micelles by the encapsulation of $^{111}In$ and $^{67}Ga$ and (4) study the biodistribution of radiolabeled polymeric micelles.

# 2 Experimental procedures

### 2.1.1 Solvents and Reagents

All the chemical reagents and solvents were of reagent grade and used without further purification unless otherwise stated.

- Dimethylformamide (DMF);
- Dichloromethane (DCM);
- Acetonitrile (ACN);
- Chloroform ($CHCl_3$);
- Water ($H_2O$): the water used was ultrapure water by Water Purification Systems – Milli-Q;
- Phosphate Buffer saline (PBS): for the experiments the concentration of the buffer was 0.01M and the pH=7.4;
- Trifluoroacetic Acid (TFA) Solution 0.1%: prepared by using 500 µL of TFA and 500 mL of Milli-Q water;
- Me-PEG-*b*-PCL: polymer used to produce the micelles. It was synthesized previously in C2TN. The molecular weight of the polymer is 10,000 Da[38];
- TBA[$Au(cdc)_2$]$^-$: compound in study. It was also synthesized and characterized previously in C2TN[36].

### 2.1.2 UV-Vis Spectroscopy

Spectra of UV-Vis were obtained in a spectrophotometer Cary 60 UV/VIS (*Agilent-Technologies*) by using quartz cuvettes (QS High Precision Cell; 10mm (*Hellma® Analytics*)). The UV-Vis Spectroscopy was used to calculate the concentration of $[Au(cdc)_2]^-$ inside the micelles after their preparation and disassembly. the UV-Vis absorption of sample solutions was recorded at $\lambda_{max}$=303 nm. The amount of $[Au(cdc)_2]^-$ was calculated using a standard calibration curve established for this compound (Figure 17).

### 2.1.3 High-Performance Liquid Chromatography (HPLC)

The HPLC analysis was conducted in a modular equipment composed by a Perkin Elmer Series 200 Pump coupled to a Perkin Elmer Series 200 UV/VIS Detector using as eluents 0.1% trifluoroacetic acid (TFA) in $H_2O$ (**A**) and acetonitrile (**B**). The eluents were HPLC grade and ultrapure milli-Q water was used to prepare the aqueous solutions. The chromatography conditions are the following:

**Column:** SUPELCO Analytical; Discovery® BIO Wide Pore 300 Å, C18; 25cm x 4.6mm, 5µm (*Sigma-Aldrich®*).

**Flow:**1.0 mL/min

**UV Detection**: $\lambda_{max}$=303 nm

**Eluents:** A – TFA 0.1% aq.; B – ACN

**Methods:** The method had the duration of 15 minutes and the gradient of solvent B was 40 – 90% (Table 2).

**Table 2 – Method with the 15 minutes of duration, being A the TFA and B the ACN.**

| Step | Time (min) | Flow (mL/min) | %A | %B |
|---|---|---|---|---|
| 0 | 0 | 1 | 60 | 40 |
| 1 | 15 | | 60 →10 | 40→90 |

## 2.1.4 Preparation of Micelles

The micelles with the complex $[Au(cdc)_2]^-$ encapsulated (BCM-$Au(cdc)_2$) were synthesized by the thin-film hydration method (Figure 8)[38]. For this method is necessary to use a round-bottom flask, so the film can be made after the removal of organic solvent.

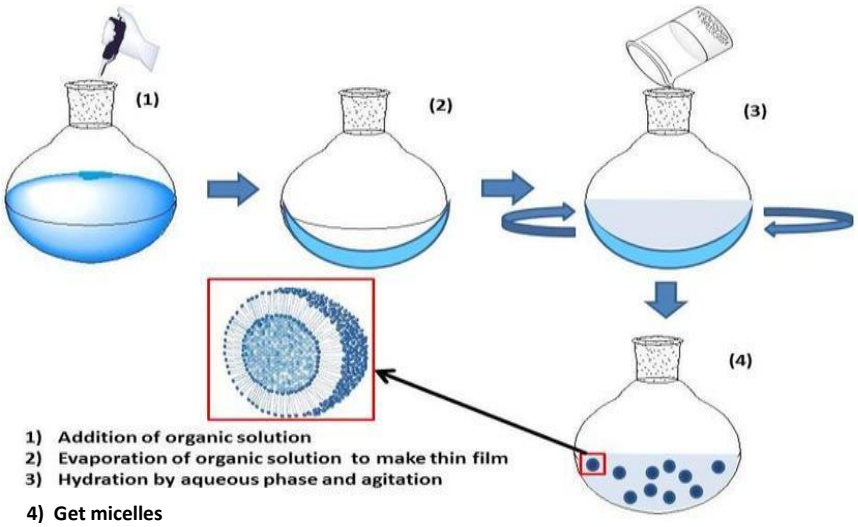


**Figure 8 – Thin-film hydration method[39].**

*General procedure:*

The first step of the method was the dissolution of the polymer (50 mg), Me-PEG-*b*-PCL, and $[Au(cdc)_2]^-$ (2 – 8 mg) in $CHCl_3$ (4 mL), under constant stirring for 4 hours at atmospheric pressure and room temperature (RT). Then, the solvent was slowly evaporated overnight under a flux of $N_2$ in order to form the $[Au(cdc)_2]^-$ / Me-PEG-b-PCL thin-film, which was hydrated at 60 ºC with $H_2O$ (or PBS) (1 mL) and stirred (low velocity) for 4 hours at RT. After the hydration, the solution was centrifuged for 10 minutes at 10000g and the supernatant was filtered by a SARTORIUS filter of 0.22 µm. The last step of this process was the lyophilization of the micelles.

### 2.1.5 Drug Loading Content and Efficiency

The drug loading content (LC) was determined by UV-Vis Spectroscopy with reference to a standard calibration curve (Figure 17). In order to do this study, 2 – 4 mg of BCM-$Au(cdc)_2$ were dissolved in 1000 µL of acetonitrile, vortex and centrifuged at 3000g for 10 minutes in order to precipitate the copolymer. After that, 600 µL of the supernatant were collected and analysed by UV-Vis spectroscopy.

The $[Au(cdc)_2]^-$ loading content (LC) was calculated by equation (1):

$$LC\ (mg_{Au(cdc)2]-}/g_{BCM}) = \frac{\text{weight of } [Au(cdc)_2] \text{ in the micelles}}{\text{total weight of BCM}(Au(cdc)_2)} \quad \textbf{(1)}$$

On the other hand, the calculation of DL efficiency (LE) can be made by equation (2):

$$LE(\%) = \frac{\text{quantitiy of } [Au(cdc)_2] \text{ in the micelles}}{\text{quantity of } [Au(cdc)_2] \text{ used}} \times 100\% \quad \textbf{(2)}$$

### 2.1.6 Size and Zeta Potential of Micelles

The zeta potential and the hydrodynamic diameter ($D_h$) of micelles (0.1 g/L) were determined in 0.01 M phosphate buffer (PB) pH 7.4, using a Zetasizer Nano ZS from Malvern with zeta-potential cells. The particle size was measured three times by dynamic light scattering (DLS) at 25 °C with a 173° scattering angle, and an optic arrangement known as non-invasive back scatter (NIBS)[38].

At the beginning of this procedure the micelles were dissolved in 0.01 M phosphate buffer, pH7.4 (PB) in order to obtain 1 g/L solutions that were subsequently sonicated for 20 minutes; before using. Afterwards, the solutions were diluted and filtered using a 0.20 µm syringe filter[38].

### 2.1.7 Cells and Cell Culture Media

A2780 (cisplatin sensitive) ovarian cancer cells were purchased from Sigma-Aldrich. Cell media and media supplements were purchased from Gibco (Thermo Fisher Scientific). The cell lines were tested for mycoplasma using the LookOut® mycoplasma PCR Detection Kit.

### 2.1.8 Determination of Cytotoxic Activity

The cytotoxic activity of BCMs, $[Au(cdc)_2]^-$ and BCMs-$Au(cdc)_2$ was evaluated with the cisplatin-sensitive A2780 cell line. Cells were grown in RPMI medium supplemented with 10% FBS and maintained in a humidified incubator (Heraeus, Germany) with 5% $CO_2$. The MTT assay was used to assess the cellular viability as a function of redox potential, i.e., metabolic active cells convert the water-soluble MTT to an insoluble purple formazan. For the assays, cells (1-2×$10^4$ cells/200 µL medium) were

seeded in 96-well plates and allowed to adhere for 24 h. Loaded BCMs (complex loading content of 3.56%) were diluted to prepare serial concentrations in the range 10 ng/mL-2g/mL a concentration that correspond to $10^{-7}$-$10^{-4}$ M of $[Au(cdc)_2]^-$. Unloaded BCMs were diluted in medium to prepare serial concentrations in the range 10 ng/mL-2 mg/mL. Loaded and unloaded micelles were added to the cells and incubated for 48 h at 37 ºC. At the end of the treatment, the medium was discarded and 200 µL of MTT solution in PBS (0.5 mg/mL) were added to each well. After 3 h at 37 °C, the medium was removed and DMSO (200 µL) was added to the cells to solubilize the formazan crystals. The percentage of cellular viability was assessed measuring the absorbance at 570 nm using a plate spectrophotometer (Power Wave Xs, Bio-Tek). The $IC_{50}$ values were calculated using the GraphPad Prism software (version 5.0). Results are shown as the mean ± SD of at least two experiments done with six replicates each.

## 2.1.9 Formation of Radiolabeled Micelles

The manipulation of all radioactive compounds was performed in a dedicated laboratory following the radiation protection rules. Activities were measured in ionization chamber (CRC-55tW by *CRC® - R Chamber)*, or in a gamma counter (Berthold, LB2111, Germany) for lower activities (< 37 kBq).

In the present study, the polymeric micelles were radiolabeled with $^{111}$In and $^{67}$Ga by encapsulation of a lipophilic radioactive compound, $^{111}$In-oxine and $^{67}$Ga-oxine, respectively.

### 2.1.9.1 $^{111}$In-BCMs

*Synthesis and characterization of $^{111}$In-oxine*

The first step was the reaction between 100 µL of oxine (8-hydroxychinolin, purity 99%, molecular weight 145.16, *E Merck Ag Darmstadt)* in ethanol (2 mg/mL) with 400 µL of sodium acetate buffer (pH 5, 0.4 M) and 100 µL of $^{111}InCl_3$ (111 MBq) in 0.01 M HCl. This reaction occurred at room temperature for 5 minutes and allowed the formation of $^{111}$In-oxine. Afterwards, 500 µL of dichloromethane was used to extract the complex $^{111}$In-oxine, because the complex is soluble in DCM. The collected activity was measured on ionization chamber (CRC-55tW by *CRC® - R Chamber*). The purity of the extracted complexes was evaluated by ITLC-SG using a mixture of $CHCl_3$/MeOH (90:10) as eluent (Rf ($^{111}$InCl3) = 0.0, Rf ($^{111}$In-oxine) = 0.9 - 1).

*Preparation of $^{111}$In-BCM*

To the solution of $^{111}$In-oxine in DCM, 1.5 mg of polymer (Me-PEG-b-PCL) was added and after that the solvent was evaporated under a flux of $N_2$. PBS (500 µL) was added to the thin-film, which resulted from the evaporation, and then the solution was put in the ultrasounds, under stirring, for 20 minutes at 35ºC.

After the formation, the radiolabeled micelles ($^{111}$In-BCM), were purified using Amicon ultra centrifugal filters (0.5 m; MWCO 10 kDa). Briefly, the solution containing the $^{111}$In-BCM was introduced in the selected Amicon filter and centrifuged during 10 minutes at 14000 rcf. Subsequently, 300 µL of PBS was added to the filter and a second centrifugation was performed using the same conditions. Finally, efficient recovery of the concentrated $^{111}$In-BCM (retained species) was achieved by a convenient reverse spin step, after collecting the filtrate. Briefly, the Amicon filter containing the purified radiolabeled micelles was inverted in a new tube and one last centrifugation was performed during 2

minutes at 2000 rcf. Once again, the activity of the solution recovered from the filter ($^{111}$In-BCM) and the filtrate ($^{111}$In-oxine) were measured and the radiolabeling yield was calculated.

The final step was the study of the *in vitro* stability of the radiolabeled micelles. For this, the $^{111}$In-BCMs were diluted in 0.1 M PBS pH 7.4 and incubated at 37 ºC. Aliquots taken at different time points were submitted to ultrafiltration using Amicon filters and the radioactivity of the filter and the filtrate were measured and used to calculate the activity retained in the micelles.

#### 2.1.9.2 $^{67}$Ga-BCMs

*Synthesis and characterization of $^{67}$Ga-oxine*

The radiopharmaceutical $^{67}$Ga-citrate was used as precursor to prepare the $^{67}$Ga-oxine lipophilic complex.

The complex mentioned above was formed by the reaction between 600 µL of $^{67}$Ga-citrate, which has the buffer incorporated, and 100 µL of the oxine solution. The reaction happened at room temperature for 5 minutes. Afterwards, 600-700 µL of dichloromethane was used to extract the complex $^{67}$Ga-oxine, since the complex is soluble in DCM. The collected activity was measured in an ionization chamber (equipment: CRC-55tW by *CRC® - R Chamber*). The purity of the extracted $^{67}$Ga-oxine was evaluated by ITLC-SG using a mixture of $CHCl_3$/MeOH (90:10) as eluent (Rf ($^{67}$Ga-citrate) = 0.0, Rf ($^{67}$Ga-oxine) = 0.9 -1).

*Preparation of $^{67}$Ga-BCM*

To the solution of $^{67}$Ga-oxine in DCM, 1.0 – 1.5 mg of polymer (Me-PEG-b-PCL) was added and after that the solvent was evaporated under a flux of $N_2$. PBS (500 µL) was added to the thin-film, which resulted from the evaporation, and then the solution was put in the ultrasounds, under stirring, for 20 minutes at 35ºC.

The micelles radiolabeled with $^{67}$Ga ($^{67}$Ga-BCM), were purified using Amicon ultra centrifugal filters (0.5 mL; MWCO 10 kDa) as above described for the $^{111}$In-BCMs. Once again, the activity of the solution recovered from the filter ($^{67}$Ga-BCM) and the filtrate ($^{67}$Ga-oxine) were measured and the radiolabeling yield was calculated.

The final step was the study of the stability of $^{67}$Ga-BCMs, that was done using the same procedure above described for the $^{111}$In-BCMs.

### 2.1.10 Efficiency of Labelling

The efficiency of labelling can be calculated based on the following equation:

$$\text{efficiency } (\%) = \frac{\text{activity of the solution recovered from the filter}}{\text{Total activity (decay corrected)}} \times 100 \quad \textbf{(3)}$$

### 2.1.11 Biodistribution

The biodistribution of $^{67}$Ga-BCMs was evaluated in groups of CD1 mice (Charles river) with seven weeks, weighting between 25 and 28 g each. Animals were injected intravenously via the tail vein with 100 µL (4.6 – 5.0 MBq) of each preparation and a normal diet ad libitum was maintained. At 4 h and 24 h post-injection (p.i.) mice were sacrificed by cervical dislocation. The radioactivity in the sacrificed mouse and the radioactive administered dose were measured in a dose calibrator (Capintec CRC25R). The difference between the radioactivity in the injected and sacrificed mouse was assumed to be due to excretion. At sacrifice, a cardiac puncture was made in order to take blood samples. Then, tissue samples of the main organs were removed, weighted and counted in a gamma counter (LB2111, Berthold, Germany). The uptake in the tissues/organs was calculated and expressed as a percentage of the injected activity per gram (%I.A./ g)[38].

The performance of all the animal experiments was made accordantly with the guidelines for animal care and ethics for animal experiments outlined in the National and European Law.

# 3 Results and Discussion

Recently, several Gold(III) complexes were screened for their antimicrobial and antitumour activities[35–37]. The monoanionic gold bisdithiolate complex, $[Au(cdc)_2]^-$ (where cdc = cyanodithioimido carbonate) (Figure 9) showed cytotoxic activity against ovarian cancer cells sensitive (A2780) and resistant (A2780cisR) to cisplatin[36]. In addition, it presented a significant antimicrobial activity towards the fungal pathogen *C. glabrata* and towards the Gram-positive *S. aureus*[36]. Hence, the therapeutic potential of $[Au(cdc)_2]^-$ should be further explored. Since $[Au(cdc)_2]^-$ exhibits poor water solubility the design of a micellar system for drug delivery of this complex was considered.

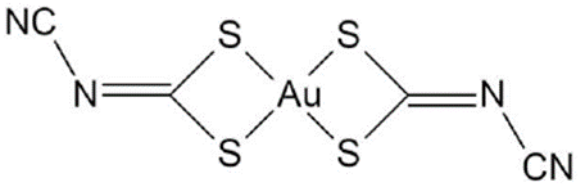


**Figure 9 – Molecular structure of complex $[Au(cdc)2]^-$ (where cdc = cyanodithioimido carbonate).**

The $[Au(cdc)_2]^-$ was kindly provided by Dulce Belo of C²TN/IST. Before the preparation of the micelles loaded with $[Au(cdc)_2]^-$, the complex was analysed by UV-Vis spectroscopy and high-performance liquid chromatography (HPLC) coupled to a UV-Vis detector. The UV-Vis spectra of complex $[Au(cdc)_2]^-$ in acetonitrile was collected and is presented in Figure 10. The maximum wavelength ($\lambda_{max}$ = 303 nm) was selected for the detection in the HPLC analysis.

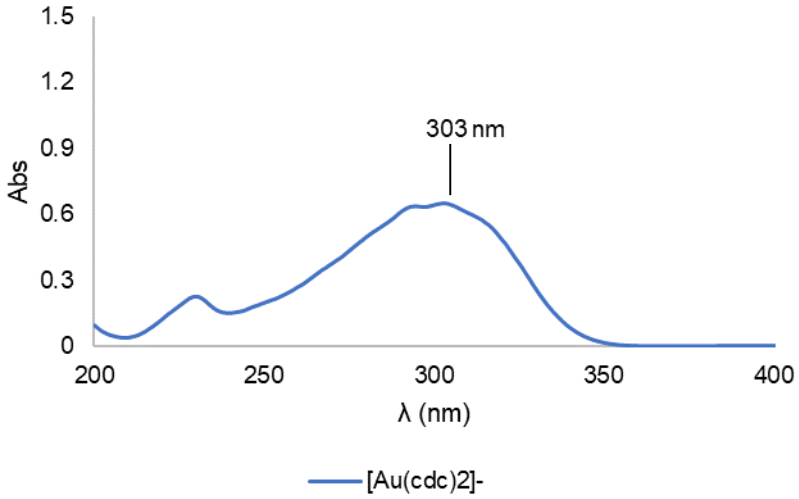


**Figure 10 – UV-Vis spectra of complex $[Au(cdc)_2]^-$ in acetonitrile.**

The gold complex $[Au(cdc)_2]^-$ dissolved in acetonitrile was then analysed by HPLC to evaluate the chemical purity and having in mind the need to evaluate the stability of the complex in the micellar formulation, including all the process for the micellar preparation, purification and lyophilization. The HPLC analysis of $[Au(cdc)_2]^-$ was performed in a $C_{18}$ column using aqueous TFA (0.1%) and acetonitrile as eluents and the detection was done at 303 nm, selected by the UV-Vis spectra previously recorded.

The $[Au(cdc)_2]^-$ complex present a high chemical purity as can be seen in the HPLC chromatogram (Figure 11) showing mainly one intense peak (Rt = 12.11 min, Table 8).

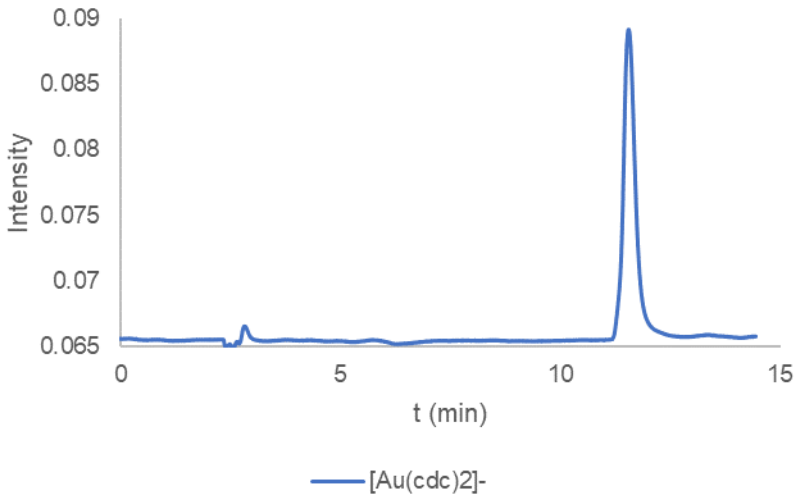


**Figure 11 – Chromatogram of $[Au(cdc)_2]^-$ on HPLC with a retention time of 12.11 minutes.**

It is well reported in the literature[9,11,13] that micelles based on the PEG-*b*-PCL block copolymers are among the best candidates for application as drug delivery systems. PEG-*b*-PCL is an amphiphilic block that self assembles into micelles in water where the hydrolytically stable hydrophilic PEG segment forms the exterior corona and the core contains the hydrophobic degradable PCL block. On that basis, the Me-PEG-*b*-PCL copolymer was selected to prepare block copolymer micelles loaded with the monoanionic gold bisdithiolate complex $[Au(cdc)_2]^-$ for drug delivery. The Me-PEG-b-PCL copolymer (Figure 12) was already synthesized in the RSG (Radiopharmaceutical Sciences Group- $C^2$TN-IST) using metal-free cationic ring-opening polymerization of ε-caprolactone (CL). The molecular weight (10000 Da) and chemical composition of the Me-PEG-b-PCL copolymer were determined based on the known molecular weight of the PEG precursor (5000 Da) and by $^1$H-NMR to calculate number of CL monomers (ca. 45).

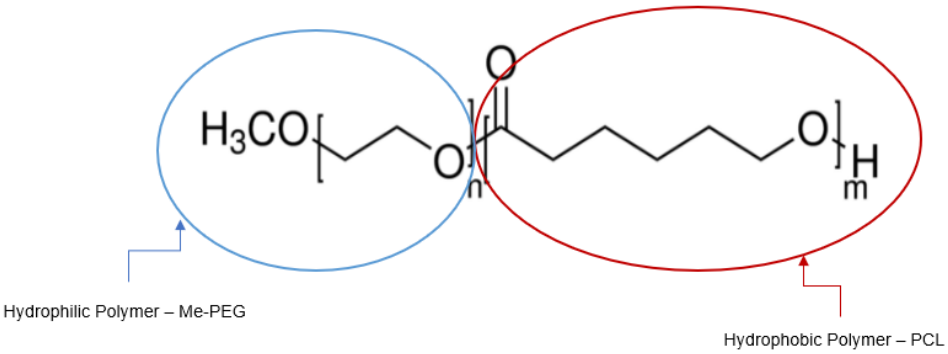


**Figure 12 – Molecular structure of Me-PEG-b-PCL[40].**

***Synthesis of Au-loaded micelles: BCM-Au(cdc)$_2$***

The synthetic pathway to prepare unloaded and Au-loaded micelles (BCM-Au(cdc)$_2$) is depicted in Figure 13. In this figure it is possible to observe that the compound is inside the formed micelle, because, as mentioned before, the compound is not soluble in water, and there is a good compatibility between the hydrophobic core and the $[Au(cdc)_2]^-$ [4,13].

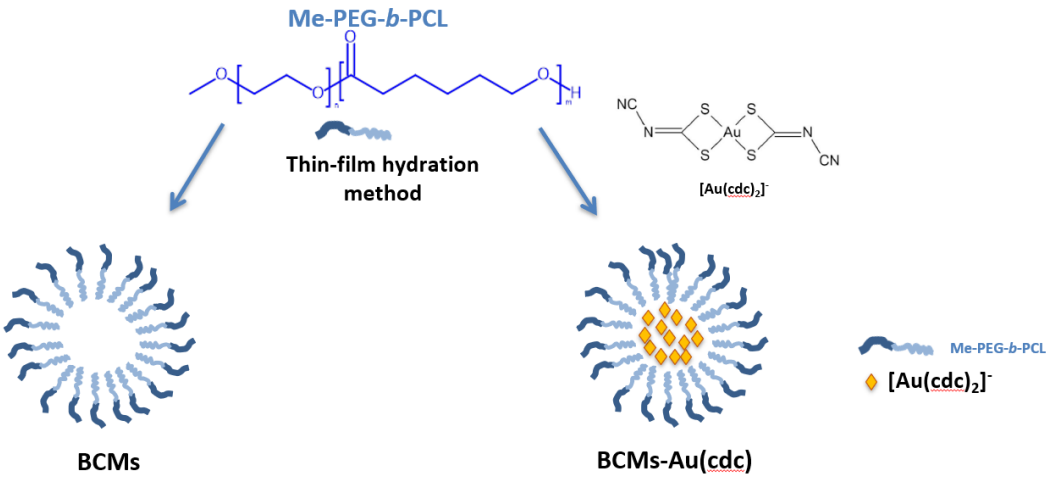


**Figure 13 – Synthesis of BCM-Au(cdc)2 by the thin-film hydration method. Non-loaded BCMs were also prepared following the same methodology, but without adding *the gold complex*. The light blue section represents the hydrophobic PCL block and the dark blue section represents the hydrophilic PEG block.**

## 3.1 Optimization of micelles loaded with $[Au(cdc)_2]^-$

The research group where this work has been performed (Radiopharmaceutical Sciences group of C$^2$TN/IST), previously prepared docetaxel loaded micelles (DTX-BCMs)[38] using the same copolymer of this present study. On their protocol, Me-PEG-b-PCL copolymer and DTX were dissolved in DMF which was then evaporated to leave a film in the bottom of a vial to be used. Warm phosphate buffer was then added with agitation and the loaded micelles (DTX-BCMs) were formed by self-assembly of the copolymer. A similar method was performed in this experiment as mentioned before in *Preparation of Micelles*. The micelles were centrifuged at 10000g and the supernatant was filtered by a SARTORIUS filter of 0.22 µm. Finally, the micelles were lyophilized.

However, for each drug to be encapsulated is necessary to optimize several parameters such as the best solvent to be used, relative amount of copolymer and drug, time and temperature, to obtain loaded micelles with high loading content and adequate properties.

### 3.1.1 First Part of the Optimization Process

The first part of the optimization for this process was made in order to select the best solvent to use for the dissolution of the gold compound and copolymer and the aqueous solution for the hydration of the thin-film. For the optimization, five different formulations were prepared using the parameters presented in Table 3.

**Table 3 – Formulations prepared for the optimization of micelles loaded with $[Au(cdc)_2]^-$.**

| | $m_{Au(cdc)2}$ (mg) | $m_{polymer}$ (mg) | Solvent for the dissolution of $Au(cdc)_2$ | Solvent for the hydration of the thin-film |
|---|---|---|---|---|
| **AS1** | 2 | 25 | DMF + DCM | PBS |
| **AS2** | | | ACN | $H_2O$ |
| **AS3** | | | ACN | PBS |
| **AS4** | | | $CHCl_3$ | $H_2O$ |
| **AS5** | | | $CHCl_3$ | PBS |

For all the studies the amount of compound and polymer was the same, 2 mg and 25 mg, respectively, so it was possible to compare the results. In addition, the volume of solvent for the dissolution was between the range of 2-4 mL and for the hydration of the thin-film (Figure 14) only 1 mL was used.

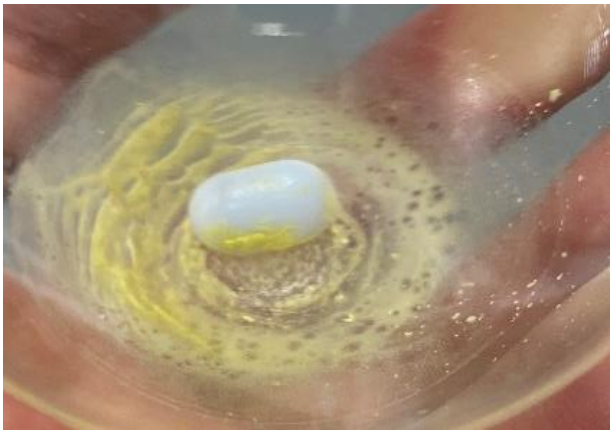

**Figure 14 – Thin-film obtained before hydration.**

All the lyophilized micelles (AS1-AS5) were analysed to determine the loading efficiency and the loading content and to evaluate the stability of the gold complex during all the process (formation of the micelles, purification and lyophilization). For this, it was necessary to do the disassembly of the micelles – a known amount of freeze-dried sample of BCMs-$Au(cdc)_2$ was dissolved in a known volume of acetonitrile and then the solution was vortexed and centrifuged to separate the gold complex from the copolymer. The UV-Vis spectra of the recovered gold complex, in acetonitrile were recorded for all the formulations and compared with the spectra obtained for the fresh solution of gold complex in acetonitrile (Figure 10). Moreover, the supernatant was also analysed by HPLC using the same method developed for the $[Au(cdc)_2]^-$ and the chromatograms were compared with the chromatogram obtained for the gold complex presented in Figure 11. As an example, the HPLC chromatogram obtained for the formulation AS4 is presented in Figure 18.

All the micelles studied have the gold complex encapsulated, with the exception of AS2, since all the spectra display a similar spectra profile as the spectrum obtained for the $[Au(cdc)_2]^-$ in acetonitrile (Figure 10), as shown in Figure 15. A new absorption band appeared below 230 nm that was ascribed to the interaction with the medium.

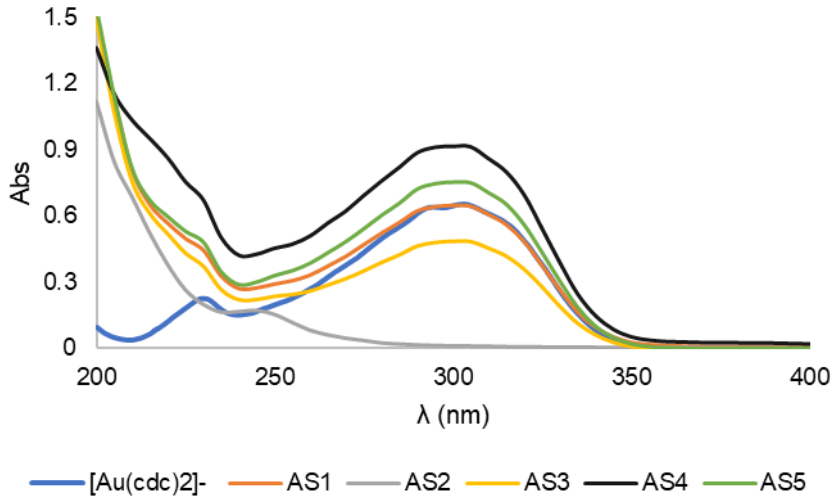


**Figure 15 – Spectra of $[Au(cdc)_2]^-$ and the micelles prepared for the optimisation process.**

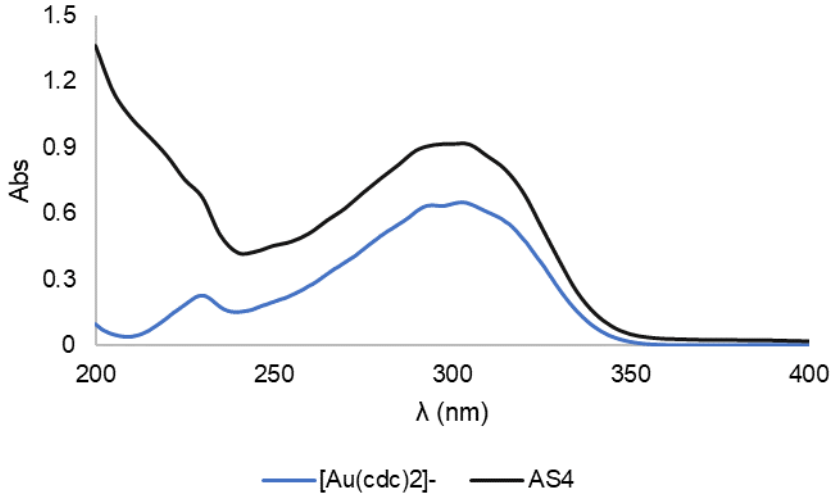


**Figure 16 – Comparison of $[Au(cdc)_2]^-$ and AS4.**

As mentioned before, studies in HPLC were also conducted. Retention times ($t_r$) – time from the injection of the sample to the time of the elution of the compound[41] – and the profile of the chromatograms were analysed to evaluate the purity of the encapsulated gold complex .

The HPLC analysis indicate that the complex remains stable in all the formulations since only one peak was observed in the HPLC chromatograms with a similar retention time as obtained in the HPLC analysis of a fresh solution of the complex $Au(cdc)_2$ in acetonitrile (Table 4).

**Table 4 – Retention times for the 15 minutes method.**

| | $t_r$ (min) |
|---|---|
| **$[Au(cdc)_2]^-$** | 12.11 |
| **AS1** | 11.90 |
| **AS2** | - |
| **AS3** | 11.63 |
| **AS4** | 12.20 |
| **AS5** | 12.27 |

The quantification of the $[Au(cdc)_2]^-$ was made by using a standard calibration curve established for the gold compound (Figure 17) (*vd Appendix A* to consult the values).

It is important to mention that the values outside this curve cannot be used, since results will have errors associated. In order to overcome this situation, for values higher than 0.02 mg/mL it is necessary to do a dilution.

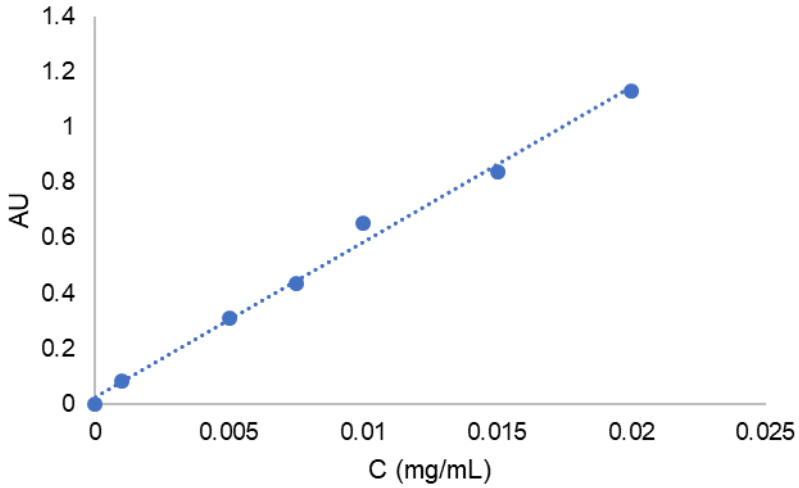


**Figure 17 – Standard calibration curve of $[Au(cdc)_2]^-$ at $\lambda_{max}$=303 nm.**

LC ($mg_{[Au(cdc)2]-}/g_{BCM}$) and LE(%) were calculated using equation (4), which has the best fit to the values of the calibration curve. This equation was calculated in *Excel* with the option *Regression* in *Data Analysis* (*vd Appendix B)*. The results are reported in Table 5.

$$Abs = 56.009 \times C + 0.0247 \quad \textbf{(4)}$$

$$R = 0.997$$

**Table 5 – Results of the micelles studied.**

| | $m_{[Au(cdc)2]-}$ (mg) | $m_{BCM}$ (mg) | LC ($mg_{Au(cdc)2]-}$ /$g_{BCM}$) |
|---|---|---|---|
| **AS1** | 0.145 | 34.5 | 4.21 |
| **AS2** | 0.000 | 5.9 | 0.00 |
| **AS3** | 0.070 | 22.8 | 3.05 |
| **AS4** | 0.096 | 16.9 | 5.68 |
| **AS5** | 0.118 | 22.4 | 5.27 |

Except for AS2, all the other micelles (AS1, AS3 - AS5) have gold compound encapsulated; however, AS3 has the lowest amount, which can mean that acetonitrile is not a good solvent for the dissolution of the copolymer and the gold compound, since in AS2 acetonitrile was also used. On the other hand, micelles in which the polymer and $[Au(cdc)_2]^-$ were dissolved with chloroform have the highest concentration of gold complex trapped in the micelles, so it is possible to conclude that $CHCl_3$ is a better solvent to prepare the micelles. In addition, the highest concentration is obtained using water during the hydration of the thin-film (AS4, Figure 16).

To summarize, among the tested solvents chloroform is the best for the dissolution of the copolymer and gold compound. Also, water seems to be better than PBS for the hydration of the thin-film, since AS4 has the higher loading content.

As mentioned before, AS4 is the best formulation of micelles, since it has the highest loading content, so it is important to compare the chromatogram obtained after the disassembly of these micelles to the one obtained for $[Au(cdc)_2]^-$, to verify if the compound undergoes, or not, degradation after encapsulation. The profile of the two chromatograms is similar, which indicates that the compound was encapsulated, and no degradation was verified (Figure 18).

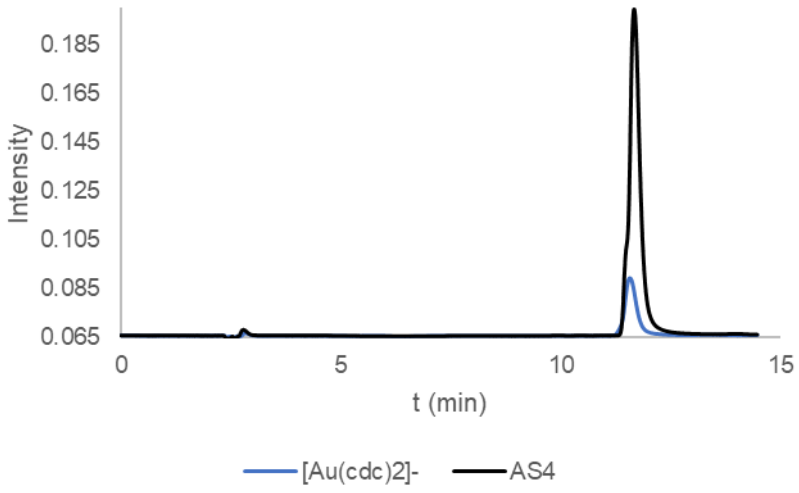


**Figure 18 – Chromatogram of $[Au(cdc)_2]^-$ *vs* AS4.**

### 3.1.2 Second Part of the Optimization Process

Taking the previous results into consideration. chloroform was the selected solvent to be used. However, the ratio drug/copolymer also impacts the achieved loading content. For the second part of the optimization, it was necessary to study the amount of $[Au(cdc)_2]^-$ needed in order to have the highest drug loading content and loading efficiency. For this, the amount of copolymer was constant, 50 mg, and the amount of gold complex varied between 1-8 mg, as seen in Table 6

The LC ($mg_{[Au(cdc)2]-}/g_{BCM}$) and LE (%) were determined as previously described for the Au-loaded micelles, AS1-AS5. On the other hand, Table 7 indicates the amount of $[Au(cdc)_2]^-$ encapsulated and weight of micelles formed for each formulation (AS6-AS9), which are necessary for the calculations of LC and LE.

**Table 6 – Values of the second optimization.**

| | solvent | $m_{polymer}$ (mg) | $m_{[Au(cdc)2]}$ (mg) | LE (%) | LC ($mg_{Au(cdc)2]-}/g_{BCM}$) |
|---|---|---|---|---|---|
| **AS6** | $CHCl_3$ | 50 | 2 | 64.59 | 35.29 |
| **AS7** | | | 4 | 7.81 | 8.47 |
| **AS8** | | | 8 | 3.34 | 7.11 |
| **AS9** | | | 1 | 65.68 | 24.25 |

**Table 7 – Values of the $[Au(cdc)_2]^-$ encapsulated and micelles formed.**

| | $m_{[Au(cdc)2]-}$ (mg/mL) | $m_{BCM}$ (mg) |
|---|---|---|
| **AS6** | 1.292 | 36.6 |
| **AS7** | 0.328 | 38.7 |
| **AS8** | 0.264 | 37.1 |
| **AS9** | 0.723 | 29.8 |

AS6 and AS9 have the major LC and LE when compared to the other two formulations, so it is possible to conclude that the drug loading content and efficiency are higher for lower quantities of $[Au(cdc)_2]^-$ (for a constant value of copolymer). In order to choose the best formulation of BCM-$Au(cdc)_2$, the LC of AS6 and AS9 were compared. As it possible to verify in Table 6, AS6 has the higher value (35.29 *vs* 24.25 mg $_{Au(cdc)2]-}/g_{BCM}$), so the optimal amount of the gold compound is 2 mg *vs* 50 mg of Me-PEG-b-PCL.

All the formulations of micelles (AS6 – AS9) were analysed by HPLC to evaluate the stability of the encapsulated gold compound. The methodology previously described for AS1-AS5 was used and the observed retention times can be found on Table 8. The $t_r$ are similar to the one determined for a fresh solution of gold complex in acetonitrile (12.11 minutes, Table 4). For comparison, the chromatogram of the gold complex incorporated in the AS6 micelles is overlaid to the chromatogram obtained with the fresh solution of $[Au(cdc)_2]^-$ in acetonitrile (Figure 19). Moreover, no further peaks were observed in any of the chromatograms indicating good stability of encapsulated gold compound, so it did not suffer any type of degradation.

**Table 8 – Residence times for the 15 minutes method on HPLC.**

| | $t_r$ (min) |
|---|---|
| **AS6** | 12.11 |
| **AS7** | 12.15 |
| **AS8** | 12.17 |

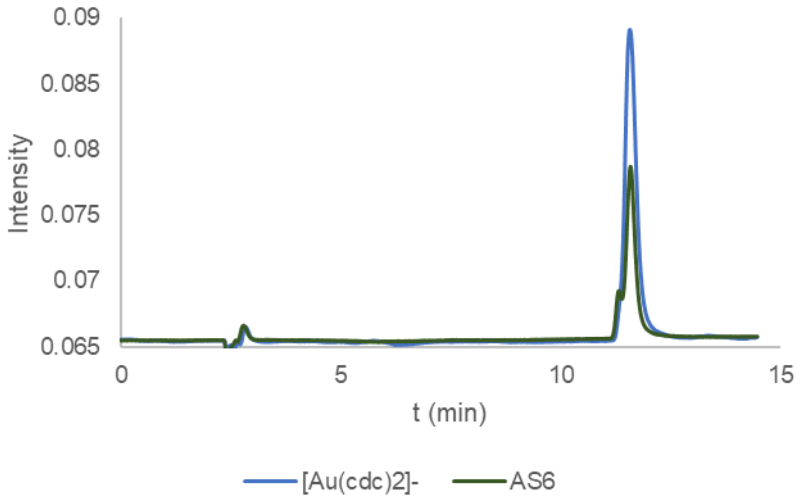


**Figure 19 – Chromatogram of $[Au(cdc)_2]^-$ *vs* AS6.**

Afterwards, the results were compared to the ones obtained for the study of auranofin-loaded nanoparticles[42], since auranofin is a gold compound in study for the treatment of bacterial infections, as $[Au(cdc)_2]^-$ [36]. The achieved drug loading content for auranofin was in the range of 1.8 – 6.2 mg[42] in comparison to 35.29 mg of $[Au(cdc)_2]^-$ per gram of micelles in formulation AS6. These results show a drug loading content higher in the $[Au(cdc)_2]^-$ loaded micelles, indicating that $[Au(cdc)_2]^-$ is encapsulated more efficiently using the optimized formulation. This is a very important achievement since a lower quantity of loaded micelles may be used to deliver the same amount of gold complex. In addition, in the experiments with the auranofin they used a different polymer – the PGLA (poly(lactic-co-glycolic acid) – instead of the Me-PEG-b-PCL. Also, the quantities used were different, in the study with auranofin they used 10-15 mg of the compound and 200 mg of PLGA and in this experiment it was used 2 mg of $[Au(cdc)_2]^-$ and 50 mg of Me-PEG-b-PCL. In order to have a good comparison the experiment should have been done with the same conditions as in the one for auranofin.

## 3.2 Size and Zeta Potential of Micelles

The hydrodynamic diameter, the PdI (polydispersity index) and the zeta potential were studied. The polydispersity index, which indicates the quality of the size of micelles[45], can vary between 0.0, which indicates that the sample is uniform with respect to the particle size, and 1.0, indicating that the sample is polydisperse, i.e. the sample has multiple particle size populations. Zeta potential is a standard characterization technique that evaluates nanoparticles surface charge which can provide

understanding into circulation times, nanoparticle stability, biocompatibility, particle cell permeability and protein interactions[46]. Absolute $Z_p$ values >30 mV are required for full electrostatic stabilization; potentials between 5 and 15 mV are in the region of limited flocculation; and for values lower than 3 mV exists the tendency to occur maximum flocculation. Hence, particle aggregation is less expected to occur for charged particles (high $Z_p$) due to electric repulsion. The nanoparticle surface can be neutral – zeta potential between -10 and +10 mV –, cationic – zeta potential greater than +30 mV – and anionic – zeta potential less than -30 mV[46,47]. In addition, zeta potential depends on the temperature, conductivity, pH and viscosity of the solvent of the host[46].

The hydrodynamic diameter ($d_h$) and the zeta potential ($Z_p$) of the micelles were determined by DLS (Dynamic Light Scattering) and LDV (Laser Doppler Velocimetry), respectively. After sample dilution with PBS (pH=7.4, 0.01 M), measurements were carried out and the values obtained for each sample are presented in Table 9.

This study was conducted on the following batches of micelles: AS1, AS4 and AS6. These micelles were chosen based on the higher loading content, previously mentioned (Table 5 and Table 6).

**Table 9 – Hydrodynamic diameter and Zeta Potential of micelles.**

| | $d_h$ (nm) | PdI | $Z_p$ (mV) |
|---|---|---|---|
| **AS1** | 50.96 ± 20.06 | 0.42 | -63.03 ± 9.75 |
| **AS4** | 70.56 ± 35.49 | 0.30 | -51.10 ± 9.92 |
| **AS6** | 77.31 ± 27.00 | 0.18 | -57.20 ± 12.10 |

Normally, polymeric micelles have a diameter in the range of 10 – 100 nm[43] and all the micelles studied have hydrodynamic diameters within this range. Also, based on the values, which are the average of the three measurements, present on Table 9, it is possible to conclude that the hydrodynamic diameter ($d_h$) is higher for micelles with a higher loading content (AS6). In addition, the micelles with the bigger $d_h$ are the ones where it was used 50 mg of polymer instead of 25 mg. Particles with a lower size than 200 nm are more likely to exhibit prolonged plasma residence time, which is a crucial feature for successful passive targeting of BCMs to solid tumours[44]. So, it can be considered that the obtained BCMs probably have an extended circulation time due to their size (<100 nm). In Figure 20 it is shown the size distribution for the first measurement of the batch AS6, as an example.

| | | | |
|---|---|---|---|
| **Sample Name:** | AS6 1 | | |
| **SOP Name:** | mansettings.nano | | |
| **File Name:** | Francisco_ITN.dts | **Dispersant Name:** | Water |
| **Record Number:** | 274 | **Dispersant RI:** | 1.330 |
| **Material RI:** | 1.50 | **Viscosity (cP):** | 0.8872 |
| **Material Absorbtion:** | 0.000 | **Measurement Date and Time:** | sexta-feira, 29 de Maio de 2020 14:... |

| | | | |
|---|---|---|---|
| **Temperature (°C):** | 25.0 | **Duration Used (s):** | 80 |
| **Count Rate (kcps):** | 146.4 | **Measurement Position (mm):** | 5.50 |
| **Cell Description:** | Clear disposable zeta cell | **Attenuator:** | 8 |

| | | | **Size (d.nm):** | **% Number:** | **St Dev (d.nm):** |
|---|---|---|---|---|---|
| **Z-Average (d.nm):** | 138.2 | **Peak 1:** | 66.14 | 100.0 | 26.17 |
| **PdI:** | 0.216 | **Peak 2:** | 0.000 | 0.0 | 0.000 |
| **Intercept:** | 0.880 | **Peak 3:** | 0.000 | 0.0 | 0.000 |

**Result quality :** Good

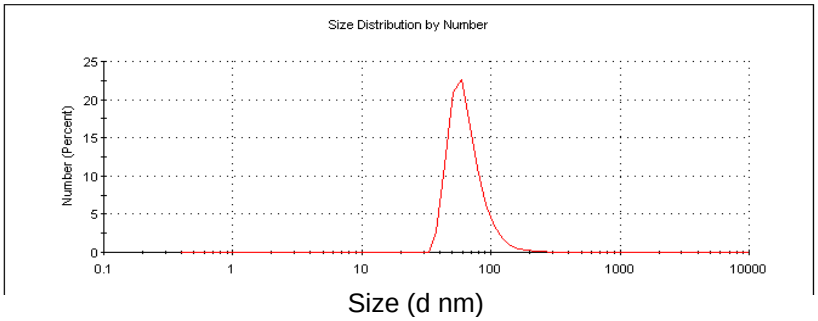


**Figure 20 – Size distribution of AS6 by DLS.**

For the PdI results, drug delivery applications using lipid-based nanocarriers, the sample is considered to be homogenous, for values of 0.3 or below[45] . In conclusion, the micelles acceptable for drug delivery are the ones from the batch AS4 and AS6 and between this two, AS6 has the best value of PdI, i.e. has the lowest value indicating that the sample is more homogenous than AS4.

The $Z_p$ analysis (Table 9) enables us to conclude that, based on absolute high $Z_p$ values (>50 mV), the micelles should not have tendency to aggregate. In this study, all the micelles formed are anionic, i.e. the surface is negatively charged, which leads to a higher rate of clearance from the blood[48]. This can be a problem since micelles have to remain in circulation for longer intervals without being taken up by the MPS in order to enter the tumour tissues through the EPR effect, as mentioned in *Passive Targeting of PMs*.

In Figure 21 it is possible to observe the zeta potential distribution for the first measurement of the batch AS6, as an example.

| | | | |
|---|---|---|---|
| **Sample Name:** | AS6 1 | | |
| **SOP Name:** | mansettings.nano | | |
| **File Name:** | Francisco_ITN.dts | **Dispersant Name:** | Water |
| **Record Number:** | 277 | **Dispersant RI:** | 1.330 |
| **Date and Time:** | sexta-feira, 29 de Maio de 2020 14:43:12 | **Viscosity (cP):** | 0.8872 |
| | | **Dispersant Dielectric Constant:** | 78.5 |

| | | | |
|---|---|---|---|
| **Temperature (°C):** | 25.0 | **Zeta Runs:** | 15 |
| **Count Rate (kcps):** | 154.7 | **Measurement Position (mm):** | 2.00 |
| **Cell Description:** | Clear disposable zeta cell | **Attenuator:** | 11 |

| | | | **Mean (mV)** | **Area (%)** | **St Dev (mV)** |
|---|---|---|---|---|---|
| **Zeta Potential (mV):** | -58.4 | **Peak 1:** | -58.4 | 100.0 | 11.7 |
| **Zeta Deviation (mV):** | 11.7 | **Peak 2:** | 0.00 | 0.0 | 0.00 |
| **Conductivity (mS/cm):** | 0.0127 | **Peak 3:** | 0.00 | 0.0 | 0.00 |

**Result quality :** Good

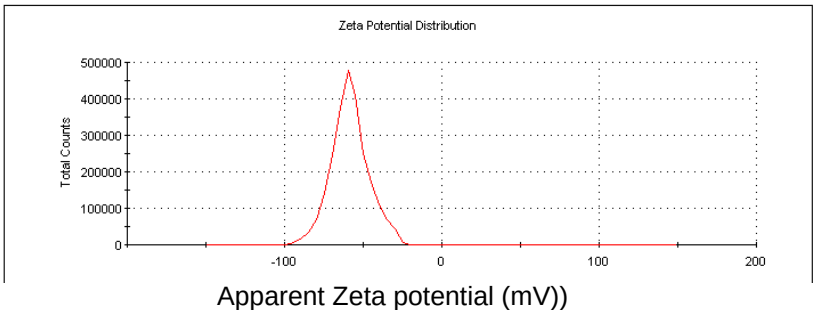


**Figure 21 – Zeta potential distribution for AS6 by LDV.**

## 3.3 Antiproliferative Activity

In a previous publication it was demonstrated that the gold complex $[Au(cdc)_2]^-$ displayed a remarkable antiproliferative activity in the ovarian cancer cell line A2780[36]. Using the colorimetric MTT assay (MTT= (3-(4,5-dimethylthiazol-2-yl)-2,5-diphenyltetrazolium bromide)) to assess the cellular viability, the $IC_{50}$ value – the concentration of complex required for 50% inhibition – was calculated after 48 hours treatment. However, as previously referred, this gold complex is water insoluble, one disadvantage for biological applications. Encapsulation of this gold complex into the block copolymer micelles was used to achieve water solubilization aiming to maintain the referred antiproliferative activity. In order to evaluate if the BCMs-$Au(cdc)_2$ are still active against the ovarian A2780 cancer cells, the MTT assay was used to compare the activity of the loaded and the unloaded BCM. Results shown in Figure 22 demonstrate that the dose response curves obtained with $[Au(cdc)_2]^-$ and BCMs-$Au(cdc)_2$ do not differ, being the $IC_{50}$ of 1.0 and 1.8 µM for $[Au(cdc)_2]^-$ and BCMs-$Au(cdc)_2$, respectively.

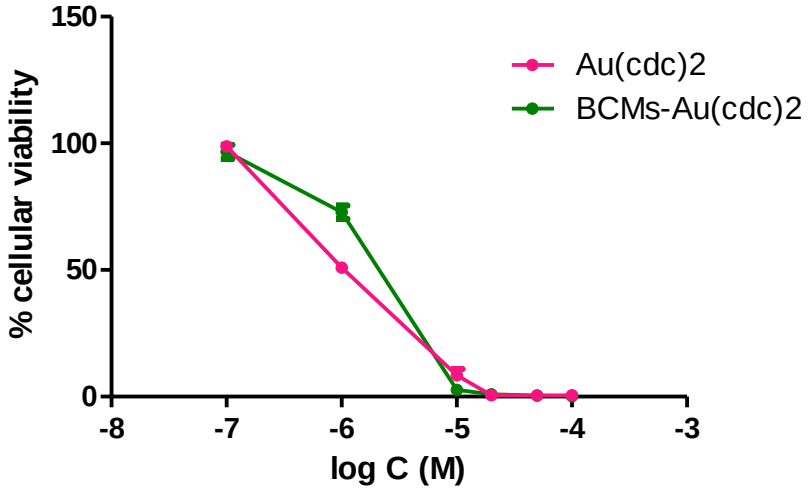


**Figure 22 – Dose-response curves found for $[Au(cdc)_2]^-$ and BCMs-$Au(cdc)_2$, using the MTT assay. The $IC_{50}$ values were calculated using the GraphPad Prism software (version 5.0). Results shown are the mean±SD of at least two experiments done with six replicates each.**

The cytotoxicity of the unloaded BCMs was also evaluated by the MTT assay. It is possible to observe in Figure 23 that only for concentrations higher than 2 mg/mL, there was *ca*. 30% loss of cellular viability. This concentration of unloaded BCMs is equivalent to that used in BCMs-$Au(cdc)_2$ for the higher concentration of $[Au(cdc)_2]^-$ (100 µM) (*Determination of Cytotoxic Activity*).

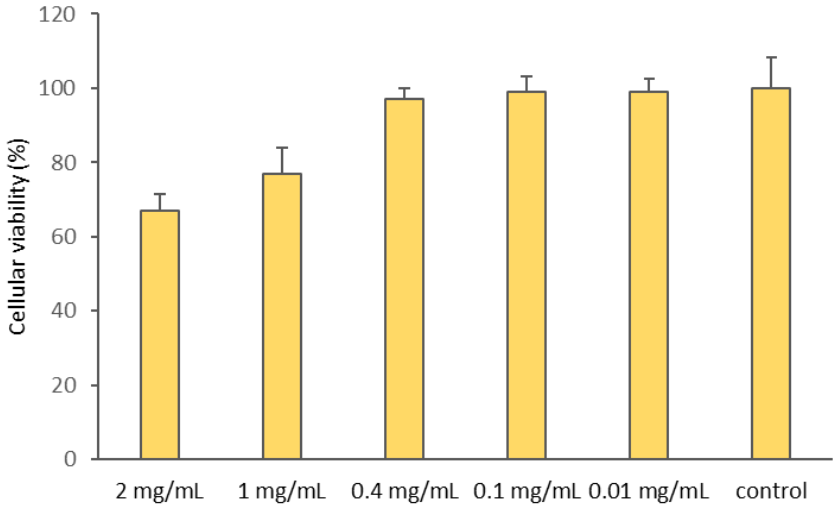


**Figure 23 – Cellular viability of A2780 cells after incubation with BCMs (unloaded micelles) for 48h. Results shown are the mean ± SD of at least two experiments done with six replicates each.**

## 3.4 Radiolabeled Micelles with $^{111}$In and $^{67}$Ga

Various factors can affect the biodistribution of polymeric micelles and it is difficult to predict the *in vivo* behaviour of new formulations, making pre-clinical evaluation essential. Nuclear methodologies offer a valuable contribution to achieve this goal, being particularly suited to provide new *in vivo*/whole body PET or SPECT imaging. To use these techniques, it is necessary to synthesise radiolabeled micelles for imaging. The radiolabeling of micelles may be accomplished using two different strategies (Figure 24):

1) Conjugation of the copolymers with an appropriate chelator or complexing agent (e.g., DOTA or DTPA) to stabilize the radiometal. Moreover, the attachment of such a chelate will modify the corona of the micelles and alter their biodistribution and pharmacokinetics.
2) A lipophilic radiolabeled compound is entrapped into the micellar core leaving the corona unaffected.

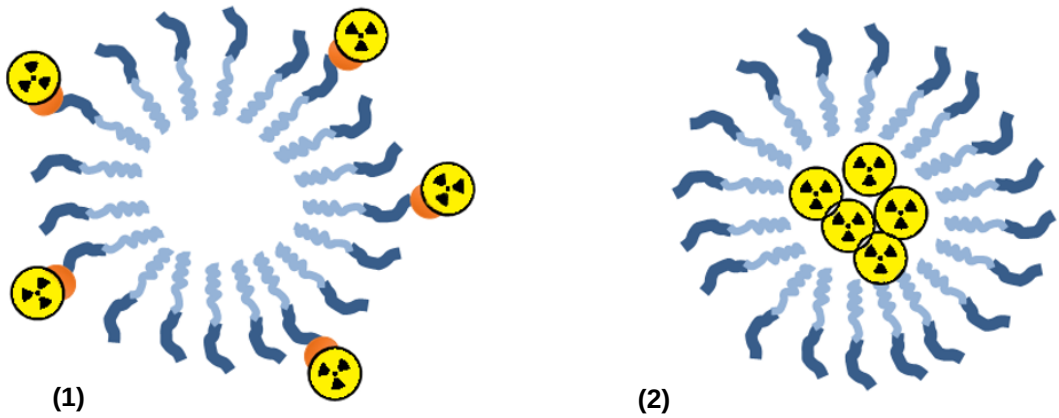


**Figure 24 – Strategies to produce radiolabeled micelles: (1) conjugation of the copolymers with an appopriate chelator or complexing agent and (2) a lipophilic radiolabeled compound is entrapped into the micellar core.**

The most explored strategy to synthesize radiolabeled micelles involved the conjugation of a copolymer functionalized with a chelator to introduce the radionuclide. Using this strategy, the RSG has prepared block copolymer micelles loaded with the chemotherapeutic docetaxel (BCM-DTX) that were radiolabeled with $^{99m}$Tc for image-guided therapy[38] or with $^{188}$Re for radiochemotherapy[49]. However, another strategy relies in the use of lipophilic radiocompounds that can be encapsulated into the micelles core. It takes advantage of the micelles capacity to spontaneously incorporate hydrophobic compounds like drugs or hydrophobic radiometal-chelate complexes. Thus, a hydrophobic *M-ligand (* means radioactive; M – metal) may be introduced into the micellar core with no requirement of previous modification of the polymers (incorporation of radionuclide or a labelled chelator). Oxine complexes of gallium radioisotopes ($^{67}$Ga, $^{68}$Ga) and $^{111}$In have been used for decades for the labeling of white blood cells. Recently, the $^{111}$In-tropolone lipophilic complex was used to radiolabel micelles by passive diffusion[50]. Based on this, a similar strategy was explored to incorporate the lipophilic complexes, $^{111}$In-oxine or $^{67}$Ga-oxine, into the micelles to prepare radiolabeled $^{111}$In-BCMs or $^{67}$Ga-BCMs, respectively.

For the radiolabeled micelles, indium-111 ($^{111}$In) and gallium-67 ($^{67}$Ga) were used. These radiometals are γ-emitters with application for SPECT imaging, with half-lifes of 2.8 ($^{111}$In) and 3.25 ($^{67}$Ga) days. In this field, their extended half-life allows them to be used as imaging agents for longer periods of evaluation after the radiopharmaceutical administration[51]. Additionally, in the particular case of gallium, it has been reported to have the ability to concentrate in certain tumours *in vivo*, inhibiting their growth[52]. It is particularly important to use long half-life radioisotopes for the labelling micelles since a prolonged circulation lifetime in the bloodstream is commonly observed for this type of particles.

*Synthesis of $^{111}$In-oxine and $^{67}$Ga-oxine*

$^{111}$In-oxine and $^{67}$Ga-oxine complexes were obtained by reaction of 8-hydroxyquinoline with the radioactive precursors $^{111}InCl_3$ or $^{67}$Ga-citrate, respectively. Both complexes, $^{111}$In-oxine and $^{67}$Ga-oxine, were obtained in high yield within 5 minutes at room temperature and were efficiently extracted to DCM (500 – 700 µL ), as mentioned in *Formation of Radiolabeled Micelles*. $^{111}$In-oxine and $^{67}$Ga-oxine, were obtained with high radiochemical purity after extraction to DCM (RCP>95 %) as determined by ITLC-SG analysis. The radiochromatogram obtained for $^{67}$Ga-oxine is presented in Figure 25.

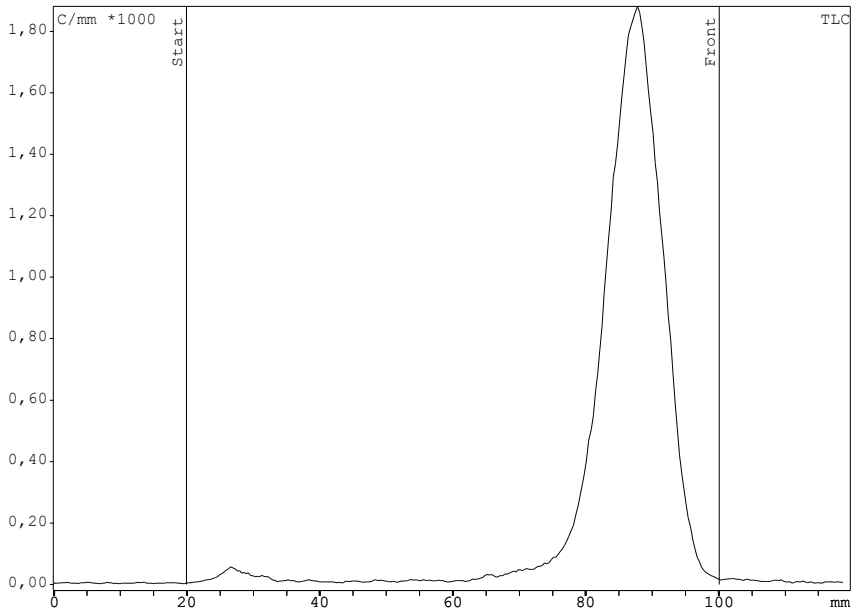


**Figure 25 – Radiochromatogram of $^{67}$Ga-oxine by ITLC-SG using as eluents $CHCl_3$/MeOH (90/10); In this chromatographic system $^{67}$Ga-citrate or $^{67}GaCl_3$ stay at origin (Rf = 0) and $^{67}$Ga-oxine migrates to the front of solvent (Rf ca 0.9).**

*Synthesis of $^{111}$In-BCMs and $^{67}$Ga-BCMs*

As mentioned in *Formation of Radiolabeled Micelles*, the copolymer Me-PEG-b-PCL was added to the purified radioactive complexes ($^{111}$In-oxine or $^{67}$Ga-oxine) in DCM. The solvent was evaporated with $N_2$ to form the thin-film that was subsquently hydrated with PBS to obtain the radiolabeled micelles ($^{111}$In-BCMs or $^{67}$Ga-BCMs). The radiolabeled micelles were purified using Amicon ultra centrifugal filters (0.5 mL; MWCO 10 kDa) to separate the unloaded radioactive-oxine complexes (Figure 26[53]). The complexes $^{111}$In-oxine and $^{67}$Ga-oxine were efficiently incorporated into the micelles leading to the formation of $^{111}$In-BCMs and $^{67}$Ga-BCMs with high yield.

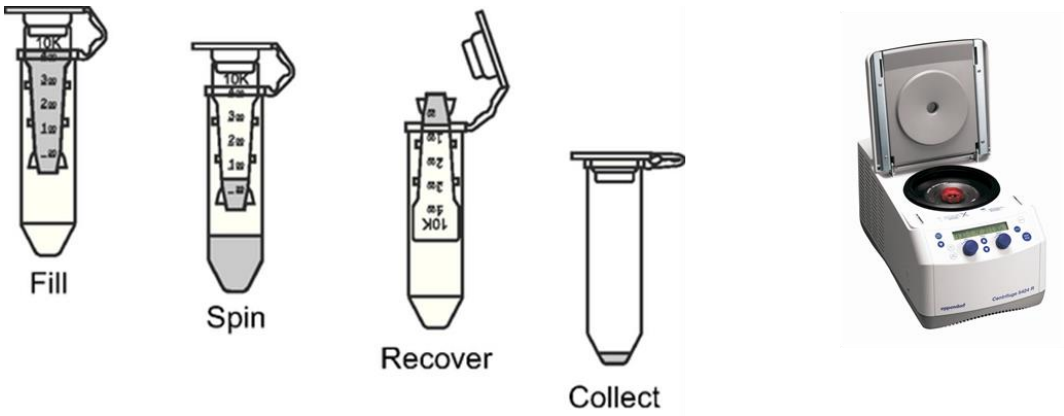


**Figure 26 – Scheme of the purification of the radiolabeled micelles to separate the unloaded radioactive-oxine complexes.**

In order to verify if the radioactive compound was encapsulated inside the micelles, it was necessary to measure the activity of the solutions after the centrifugation: filtered and the recovered solution from the filter (solution with the micelles), and also the activity adsorbed to the filter.

The results can be found on the Tables Table 10 and Table 11.

**Table 10 – Activity of $^{111}$In-BCMs.**

| | Activity (µCi) | Radiolabeling Efficiency (%) |
|---|---|---|
| **Filtered** | 4.57 | |
| **Filter** | 13.6 | 86.79 |
| **Recovered from the Filter** | 119.4 | |

**Table 11 – Activity of $^{67}$Ga-BCMs (using $^{67}$Ga-citrate to prepare the $^{67}$Ga-oxine).**

| | Activity (µCi) | Radiolabeling Efficiency (%) |
|---|---|---|
| **Filtered** | 144 | |
| **Filter** | 114.5 | 73.95 |
| **Recovered from the Filter** | 734 | |

As expected, the activity of the solution recovered from the filter (radiolabeled micelles) is higher when compared to the activity of the filtrate, which indicates that most of the quantity of the radioactive oxine ($^{67}$Ga-oxine or $^{111}$In-oxine) were encapsulated into the micelles. In addition, it is important to mention that the activity adsorbed to the filter can be neglected – activities are very low when compared to the ones of the recovered solution from the filter – meaning that the radioactive compounds are not significantly adsorbed by the filter. Also, the efficiency of labelling was calculated and as it possible to observe the values are high (> 73% for $^{67}$Ga and > 86% for $^{111}$In).

After purification by the Amicon filters, the radiolabeled micelles loaded with $^{67}$Ga-oxine or $^{111}$In-oxine ($^{67}$Ga-BCMs and $^{111}$In-BCMs) were obtained with high purity (> 95% activity retained in the micelles for both cases).

Recently, a similar methodology was described for radiolabeling polymeric micelles using $^{111}$In-tropolone to be incorporated into the micelles core.[50] However, the authors reported a lower radiolabeling yield of the micelles (34 ± 1%) in comparison to the radiolabeling yield observed by us, for $^{67}$Ga-BCMs (73.9 %) and specially for $^{111}$In-BCMs (86.8%).

*In Vitro stability studies of the radiolabeled micelles*

The *in vitro* stability of radiolabeled micelles was studied for 6 days ($^{111}$In-BCMs) and 4 days ($^{67}$Ga-BCMs) at 37°C by incubation with 0.1 M PBS buffer pH 7.4 (physiological conditions) and the results are shown in Tables 12 and 13, respectively. The release of radioactivity was measured as an indicator for the stability of the $^{67}$Ga-oxine or $^{111}$In-oxine-labeled micelles. To evaluate the release of the radioactivity from the micelles, the solutions incubated in physiological conditions were filtrated by centrifugation with Amicon filters. The activity released from the micelles was in the filtrate while the activity retained in the filter represents the activity retained inside the micelles. The activity was measured and used to calculate the % of activity inside the micelles (Table 12 and Table 13).

Once again, the activity of the recovered solution is higher when compared to the one of the filtered, so it is possible to conclude that the radiolabeled micelles are stable. The lower activity has to do with the isotope decay.

**Table 12 – Stability of $^{111}$In-BCMs, in physiological conditions (pH and temperature)**

| t (days) | Act. Filtered (µCi) | Act. Recovered Solution | |
|---|---|---|---|
| | | (µCi) | (%) |
| 2 | 0.35 | 19.84 | 98.27 |
| 6 | 0.13 | 4.06 | 96.90 |

**Table 13 – Stability of $^{67}$Ga-BCMs in physiological conditions (pH and temperature)**

| t (days) | Act. Filtered (µCi) | Act. Recovered Solution | |
|---|---|---|---|
| | | (µCi) | (%) |
| 4 | 0.27 | 6.08 | 95.83 |

## 3.5 Biodistribution

In order to have preliminary data concerning the pharmacokinetics of the radiolabeled micelles, the biodistribution was studied at 4h and 24h after administration. Biodistribution is influenced by the interactions of the micelles with the organs, which are dependent on the physical and biochemical properties of the micelles and the characteristics of the organs[54]. Once the nanocarriers are injected, they are transferred by the bloodstream and distributed to peripheral organs, and simultaneously cleared by these organs. The clearance can be hepatic (through liver), renal (through kidneys), gastric (through gastrointestinal track) or mucociliary (through lungs), depending on the properties of nanoparticles[54,55].

As mentioned before, the biodistribution was done for the $^{67}$Ga labelled micelles ($^{67}$Ga-BCMs) and the data obtained from the study are shown in Figure 27 (*vd Appendix C* in order to consult the exact values).

The uptake in the tissues was determined and presented as a percentage of the injected activity per gram of organ/tissue. (% I.A./g ± SD). The whole-body radioactivity excretion was determined as a percentage of the total injected activity. A relatively slow blood clearance was observed (7.3 ± 1.3 and 2.6 ± 1.3 % I.A./g blood at 4 h and 24 h p.i.,respectively) and is in accordance with the behaviour previously observed for micelles radiolabeled with $^{188}$Re (11.2 ± 0.9 and 4.6 ± 1.5 % I.A./g blood at 4 h and 24 h p.i., respectively)[49]. Radioactivity accumulation detected in highly irrigated organs such as lungs and heart may be attributed to the high activity in the blood pool with slow washout from these organs that clear over time.

After the 4 hours post-injection, a relevant liver uptake was found (10.9 ± 0.4 %I.A./g organ, respectively) that decreased at 24 hours p.i. (5.5 ± 1.1 % I.A./g organ, respectively), which indicates that the main route of clearance are the hepatobiliary excretory pathway. Significant kidney uptake was found (7.5 ± 0.5 I.A./g at 4 h p.i.) that was mostly retained at 24 h (4.7 ± 0.8% I.A./g) suggesting involvement of renal elimination.

The bone uptake (femur) increased after 24 hours post-injection (6.8 ± 1.0 %I.A./g organ at 4h to 9.4 ± 1.3 %I.A./g organ) which can mean that there is free $^{67}$Ga inside the body, since in previous studies[56] the uptake of free gallium-67 by the bone increased after 24 hours post-injection.

In addition, the rate of radioactivity excretion was low: 9.5 ± 2.4 %I.A. after 4 hours p.i. and 30.6 ± 2.2 %I.A. after 24 hours post-injection. This behaviour agrees with the expected distribution profile in micelle formulations.

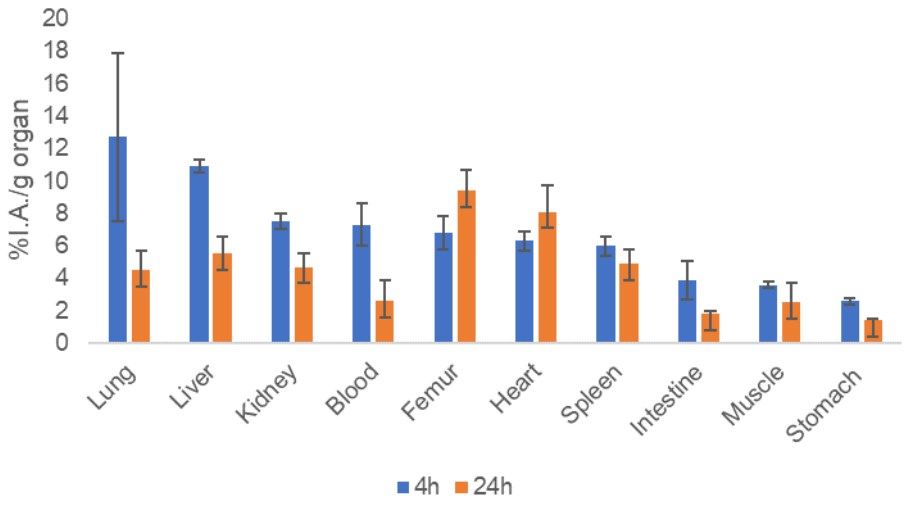


**Figure 27 – Biodistribution of $^{67}$Ga-BCMs micelles in CD1 health mice at 4h and 24h p.i., expressed as %I.A./g organ.**

# 4 Conclusions and Future Perspectives

The work developed in this thesis focused on the development of BCMs loaded with the gold complex $[Au(cdc)_2]^-$ in order to explore their therapeutic potential towards cancer cells. BCMs were synthesized using different dissolution and hydration film solvents, as well as varying ratios of polymer/$[Au(cdc)_2]^-$ complex. The one synthesized using chloroform for the dissolution, water for the thin film hydration and a polymer/$[Au(cdc)_2]^-$ ratio of 50 mg/2 mg (AS6), was the one that showed the highest drug loading efficiency and loading content (64.59%, 35.29 $mg_{[Au(cdc)2]-}/g_{BCM,}$ respectively). This loading content was high when compared to a previous study with auranofin, which LC was only 1.8 – 6.2 mg of auranofin/g of polymer[42].

AS6 had a hydrodynamic diameter of 77.31 ± 27.00 nm and a zeta potential of -57.20 ± 12.10 mV, so micelles were formed and their surface was negatively charged, which means that the rate of clearance from the blood is high what can be a problem since micelles have to remain in circulation for longer intervals without being taken up by the MPS in order to enter the tumour tissues through the EPR effect. Furthermore, the sample had a PdI of 0.18, meaning that the sample was homogenous and polymeric micelles are acceptable as drug delivery carriers.

Cytotoxic activity studies against the ovarian A2780 cancer cells sensitive to cisplatin have shown that BCMs-$Au(cdc)_2$ loaded micelles present relevant cytotoxic activity. In comparison to the free $[Au(cdc)_2]^-$ complex the loaded-micelles exhibit similar cytotoxic effect for the same concentration of gold complex, which may lead to similar therapeutic outcome with less side effects.

The formulation of radiolabeled micelles using $^{111}In$ and $^{67}Ga$ radioisotopes, was done by the encapsulation of the radioactive lipophilic compounds ($^{111}In$-oxine or $^{67}Ga$-oxine) inside the micelles. The efficiency of labelling was high (> 70% for $^{67}Ga$ and > 86% for $^{111}In$), particularly when compared to previous studies, whose efficiency achieved was only 34 ± 1% for $^{111}In$[50]. In vitro stability studies have shown that the purified $^{111}In$-BCMs and $^{67}Ga$-BCMs are stable in physiological conditions (37 °C and pH 7.4) for at least 4 days since no significant release of radioactivity was observed. Preliminary biodistribution studies with $^{67}Ga$-BCMs, performed in healthy CD1 mice, has shown a slow blood clearance and prolonged circulation lifetime in the bloodstream. However, the uptake in the bone increased overtime (6.8 ± 1.0 %I.A./g organ and 9.4 ± 1.3 %I.A./g organ, at 4h and 24h p.i., respectively) indicating a slow release of $^{67}Ga$ *in vivo*.

It should be taken into account that, due to the *Covid-19 Pandemic* some of the planned studies were not concluded.

For future studies there are some points which are important in order to enrich the experiments done, such as:

- Evaluate the *in vitro* release of $[Au(cdc)_2]^-$ from the loaded-micelles overtime in different conditions (pH 7.4 vs pH 5, both at 37 °C);
- Study the cytotoxic effect of BCMs-$Au(cdc)_2$ loaded micelles against A2780cisR cancer cells, resistant to cisplatin;
- Synthesize and biologically evaluate polymeric micelles loaded simultaneously with the gold complex $[Au(cdc)_2]^-$ and a radiocompound (*e.g.* $^{111}In$-oxine, $^{67}Ga$-oxine);
- Modify the polymer and add a specific ligand for the EGF receptor.

# 5 References


1. Khalid M. El-Say & Hossam S.El-Sawy. Polymeric nanoparticles: Promising platform for drug delivery. *Int. J. Pharm.* **528**, 675–691 (2017).

2. Jong, W. H. De & Paul, J. B. Drug delivery and nanoparticles : Applications and hazards. *Int. J. Nanomedicine* **3**, 133–149 (2008).

3. Jhaveri, A. M. & Torchilin, V. P. Multifunctional polymeric micelles for delivery of drugs and siRNA. *Front. Pharmacol.* **5 APR**, 1–26 (2014).

4. Cabral, H., Miyata, K., Osada, K. & Kataoka, K. Block Copolymer Micelles in Nanomedicine Applications. *Chem. Rev.* **118**, 6844–6892 (2018).

5. Nanotechnology in Medicine - Nanoparticles in Medicine. https://www.understandingnano.com/medicine.html.

6. What is Nanomedicine? https://etp-nanomedicine.eu/about-nanomedicine/what-is-nanomedicine/.

7. Pelaz, B. *et al.* Diverse Applications of Nanomedicine. *ACS Nano* **11**, 2313–2381 (2017).

8. Khodabandehloo, H., Zahednasab, H. & Hafez, A. A. Nanocarriers usage for drug delivery in cancer therapy. *Int. J. Cancer Manag.* **9**, (2016).

9. Lamberti, M., Zappavigna, S., Sannolo, N., Porto, S. & Caraglia, M. Advantages and risks of nanotechnologies in cancer patients and occupationally exposed workers. *Expert Opin. Drug Deliv.* **11**, 1087–1101 (2014).

10. No Title. https://www.rsc.org/cpd/teachers/content/filerepository/frg/pdf/Nanoparticles.pdf.

11. Rizvi, S. A. A. & Saleh, A. M. Applications of nanoparticle systems in drug delivery technology. *Saudi Pharm. J.* **26**, 64–70 (2018).

12. Bose, T., Latawiec, D., Mondal, P. P. & Mandal, S. Overview of nano-drugs characteristics for clinical application: The journey from the entry to the exit point. *J. Nanoparticle Res.* **16**, (2014).

13. Oerlemans, C. *et al.* Polymeric micelles in anticancer therapy: Targeting, imaging and triggered release. *Pharm. Res.* **27**, 2569–2589 (2010).

14. Yadav, H. K. S., Almokdad, A. A., shaluf, S. I. M. & Debe, M. S. *Polymer-Based Nanomaterials for Drug-Delivery Carriers*. *Nanocarriers for Drug Delivery* (Elsevier Inc., 2019). doi:10.1016/b978-0-12-814033-8.00017-5.

15. Cholkar, K., Patel, A., Dutt Vadlapudi, A. & K. Mitra, A. Novel Nanomicellar Formulation Approaches for Anterior and Posterior Segment Ocular Drug Delivery. *Recent Patents Nanomedicinee* **2**, 82–95 (2012).

16. Amin, M. C. I. M., Butt, A. M., Amjad, M. W. & Kesharwani, P. *Polymeric Micelles for Drug Targeting and Delivery*. *Nanotechnology-Based Approaches for Targeting and Delivery of Drugs and Genes* (Elsevier Inc., 2017). doi:10.1016/B978-0-12-809717-5.00006-3.

17. Xie, X. *et al.* Challenges and Opportunities from Basic Cancer Biology for Nanomedicine for Targeted Drug Delivery. *Curr. Cancer Drug Targets* **19**, 257–276 (2019).

18. Barua, S. & Mitragotri, S. Challenges associated with penetration of nanoparticles across cell and tissue barriers: A review of current status and future prospects. *Nano Today* **9**, 223–243 (2014).

19. EGF and Cancer. https://www.sinobiological.com/resource/cytokines/egf-cancer.

20. Morshed, M. & Chowdhury, E. H. *Gene delivery and clinical applications*. *Encyclopedia of Biomedical Engineering* vols 1–3 (Elsevier, 2018).

21. Lin, Y.-S., Lee, M.-Y., Yang, C.-H. & Huang, K.-S. Active Targeted Drug Delivery for Microbes Using Nano-Carriers. *Curr. Top. Med. Chem.* **15**, 1525–1531 (2015).

22. Zhou, Q., Zhang, L., Yang, T. H. & Wu, H. Stimuli-responsive polymeric micelles for drug delivery and cancer therapy. *Int. J. Nanomedicine* **13**, 2921–2942 (2018).

23. Aderibigbe, B. A. Polymeric therapeutic delivery systems for the treatment of infectious diseases. *Ther. Deliv.* **8**, 557–576 (2017).

24. Kumar, R., Kulkarni, A., Nagesha, D. K. & Sridhar, S. In vitro evaluation of theranostic polymeric micelles for imaging and drug delivery in cancer. *Theranostics* **2**, 714–722 (2012).

25. Movassaghian, S., Merkel, O. M. & Torchilin, V. P. Applications of polymer micelles for imaging and drug delivery. *Wiley Interdiscip. Rev. Nanomedicine Nanobiotechnology* **7**, 691–707 (2015).

26. Grallert, S. R. M., Rangel-Yagui, C. de O., Pasqualoto, K. F. M. & Tavares, L. C. Polymeric micelles and molecular modeling applied to the development of radiopharmaceuticals. *Brazilian J. Pharm. Sci.* **48**, 1–16 (2012).

27. Pricker, S. P. Medical uses of gold compounds: Past, present and future. *Gold Bull.* **29**, 53–60 (1996).

28. Yeo, C., Ooi, K. & Tiekink, E. Gold-Based Medicine: A Paradigm Shift in Anti-Cancer Therapy? *Molecules* **23**, 1410 (2018).

29. Berners-Price, S. J. & Filipovska, A. Gold compounds as therapeutic agents for human diseases. *Metallomics* **3**, 863 (2011).

30. Roder, C. & Thomson, M. J. Auranofin: Repurposing an Old Drug for a Golden New Age. *Drugs R. D.* **15**, 13–20 (2015).

31. Onodera, T., Momose, I. & Kawada, M. Potential Anticancer Activity of Auranofin. *Chem. Pharm. Bull.* **67**, 186–191 (2019).

32. Cassetta, M. I., Marzo, T., Fallani, S., Novelli, A. & Messori, L. Drug repositioning: auranofin as a prospective antimicrobial agent for the treatment of severe staphylococcal infections. *BioMetals* **27**, 787–791 (2014).

33. Radisavljević, S. & Petrović, B. Gold(III) Complexes: An Overview on Their Kinetics, Interactions With DNA/BSA, Cytotoxic Activity, and Computational Calculations. *Front. Chem.* **8**, (2020).

34. Kim, J. H., Reeder, E., Parkin, S. & Awuah, S. G. Gold(I/III)-Phosphine Complexes as Potent Antiproliferative Agents. *Sci. Rep.* **9**, 12335 (2019).

35. Pintus, A. *et al.* [Au(py b -H)(mnt)]: A novel gold(III) 1,2-dithiolene cyclometalated complex with antimicrobial activity (py b -H = C-deprotonated 2-benzylpyridine; mnt = 1,2-dicyanoethene-1,2-dithiolate). *J. Inorg. Biochem.* **170**, 188–194 (2017).

36. Sousa, S. A. *et al.* On the path to gold: Monoanionic Au bisdithiolate complexes with antimicrobial and antitumor activities. *J. Inorg. Biochem.* **202**, 110904 (2020).

37. Fontinha, D. *et al.* Gold( <scp>iii</scp> ) bis(dithiolene) complexes: from molecular conductors to prospective anticancer, antimicrobial and antiplasmodial agents. *Metallomics* **12**, 974–987 (2020).

38. Ribeiro, E. *et al.* Radiolabeled block copolymer micelles for image-guided drug delivery. *Int. J. Pharm.* **515**, 692–701 (2016).

39. Sun, C. BUBBLE LIPOSOME: A MODERN THERANOSTIC APPROACH OF NEW DRUG DELIVERY. *World J. Pharm. Pharm. Sci.* 1290–1314 (2017) doi:10.20959/wjpps20175-9222.

40. Methoxy poly(ethylene glycol)-block-poly(ε-caprolactone). https://www.sigmaaldrich.com/catalog/product/aldrich/900649?lang=pt&region=PT.

41. Retention Time. https://www.sciencedirect.com/topics/chemistry/retention-time.

42. Díez-Martínez, R. *et al.* Auranofin-loaded nanoparticles as a new therapeutic tool to fight streptococcal infections. *Sci. Rep.* **6**, 19525 (2016).

43. Polymeric Micelle. https://www.sciencedirect.com/topics/engineering/polymeric-micelle.

44. Lee, H. ROLES OF PASSIVELY AND ACTIVELY TARGETED BLOCK COPOLYMER MICELLES IN CANCER THERAPY. (University of Toronto).

45. Danaei, M. *et al.* Impact of Particle Size and Polydispersity Index on the Clinical Applications of Lipidic Nanocarrier Systems. *Pharmaceutics* **10**, 57 (2018).

46. Smith, M. C., Crist, R. M., Clogston, J. D. & McNeil, S. E. Zeta potential: a case study of cationic, anionic, and neutral liposomes. *Anal. Bioanal. Chem.* **409**, 5779–5787 (2017).

47. Zeta Potential. https://www.sciencedirect.com/topics/pharmacology-toxicology-and-pharmaceutical-science/zeta-potential.

48. Raza, K., Kumar, P., Kumar, N. & Malik, R. Pharmacokinetics and biodistribution of the nanoparticles. *Adv. Nanomedicine Deliv. Ther. Nucleic Acids* 166–186 (2017) doi:10.1016/B978-0-08-100557-6.00009-2.

49. Ribeiro, E. *et al.* Docetaxel-loaded block copolymer micelles labeled with 188Re for combined radiochemotherapy. *J. Drug Deliv. Sci. Technol.* **60**, 101898 (2020).

50. Laan, A. C. *et al.* Radiolabeling polymeric micelles for in vivo evaluation: a novel, fast, and facile method. *EJNMMI Res.* **6**, 1–10 (2016).

51. Psimadas, D., Georgoulias, P., Valotassiou, V. & Loudos, G. Molecular Nanomedicine Towards Cancer : *J. Pharm. Sci.* **101**, 2271–2280 (2012).

52. Chitambar, C. R. Gallium complexes as anticancer drugs. *Met. Dev. Action Anticancer Agents* **18**, 281–301 (2018).

53. No Title. https://www.merckmillipore.com/INTERSHOP/static/WFS/Merck-Site/-/Merck/en_US/Freestyle/BI-Bioscience/PSP/PSP-images/img_graphic4.jpg.

54. Wei, Y., Quan, L., Zhou, C. & Zhan, Q. Factors relating to the biodistribution & clearance of nanoparticles & their effects on in vivo application. *Nanomedicine* **13**, 1495–1512 (2018).

55. Bourquin, J. *et al.* Biodistribution, Clearance, and Long-Term Fate of Clinically Relevant Nanomaterials. *Adv. Mater.* **30**, 1–31 (2018).

56. Fazaeli, Y. *et al.* Development of ga-67 maltolate complex as an imaging agent. *Iran. J. Pharm. Res. IJPR* **11**, 755–62 (2012).

# 6 Appendix A

**Table 14 – Concentration vs absorbance.**

| C (mg/mL) | Abs |
|---|---|
| 0.0200 | 1.132 |
| 0.0100 | 0.654 |
| 0.0150 | 0.840 |
| 0.0050 | 0.309 |
| 0.0075 | 0.434 |
| 0.0010 | 0.081 |

# 7 Appendix B

SUMÁRIO DOS RESULTADOS

| *Estatística de regressão* | |
|---|---|
| R múltiplo | 0.996852357 |
| Quadrado de R | 0.993714621 |
| Quadrado de R ajustado | 0.992457545 |
| Erro-padrão | 0.035543824 |
| Observações | 7 |

ANOVA

| | *gl* | *SQ* | *MQ* | *F* | *F de significância* |
|---|---|---|---|---|---|
| Regressão | 1 | 0.998684916 | 0.998685 | 790.4969512 | 1.06582E-06 |
| Residual | 5 | 0.006316817 | 0.001263 | | |
| Total | 6 | 1.005001733 | | | |

| | *Coeficientes* | *Erro-padrão* | *Stat t* | *valor P* | *95% inferior* | *95% superior* | *Inferior 95.0%* | *Superior 95.0%* |
|---|---|---|---|---|---|---|---|---|
| Interceptar | 0.024744573 | 0.021392515 | 1.156693 | 0.29965477 | -0.030246638 | 0.079735785 | -0.030246638 | 0.079735785 |
| Variável X 1 | 56.00888745 | 1.992080326 | 28.11578 | 1.06582E-06 | 50.88808195 | 61.12969296 | 50.88808195 | 61.12969296 |

# 8 Appendix C

**Table 15 – Values of biodistribution of $^{67}$Ga-BCMs micelles in CD1 health mice at 4h and 24h p.i., expressed as %I.A./g organ.**

| | t = 4 h | t = 24 h |
|---|---|---|
| **Blood** | 7.3 ± 1.3 | 2.6 ± 1.3 |
| **Liver** | 10.9 ± 0.4 | 5.5 ± 1.1 |
| **Intestine** | 3.9 ± 1.2 | 1.8 ± 0.2 |
| **Spleen** | 6.0 ± 0.6 | 4.9 ± 0.9 |
| **Heart** | 6.3 ± 0.6 | 8.1 ± 1.6 |
| **Lung** | 12.7 ± 5.2 | 4.5 ± 1.2 |
| **Kidney** | 7.5 ± 0.5 | 4.7 ± 0.8 |
| **Muscle** | 3.6 ± 0.2 | 2.5 ± 1.2 |
| **Femur** | 6.8 ± 1.0 | 9.4 ± 1.3 |
| **Stomach** | 2.6 ± 0.2 | 1.4 ± 0.1 |
| **Excretion (%I.A.)** | 9.5 ± 2.4 | 30.6 ± 2.2 |